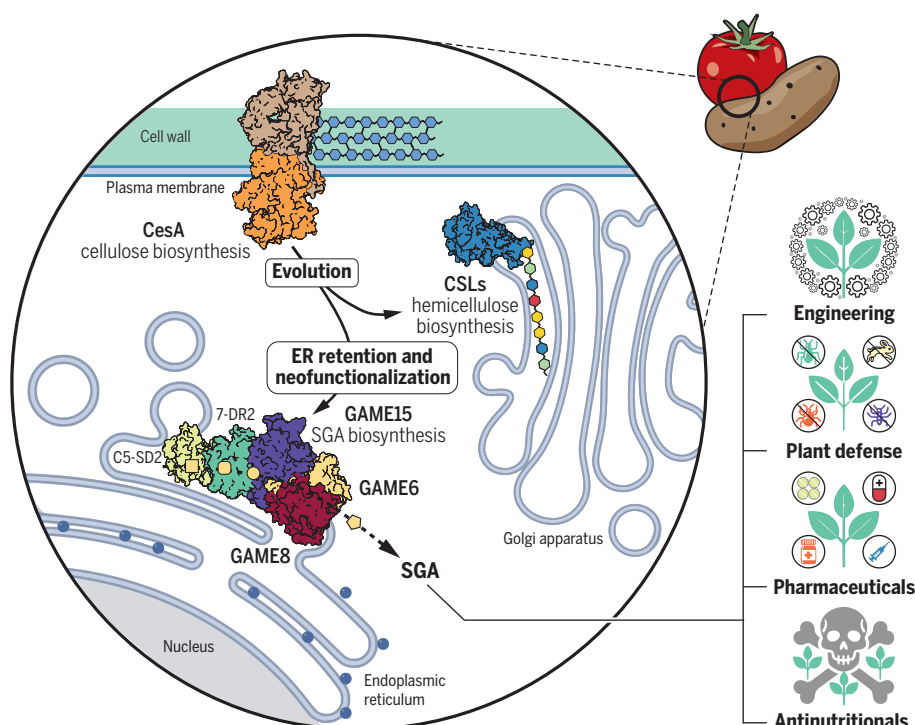## PLANT SCIENCE

A cellulose synthase–like protein governs the biosynthesis of *Solanum* alkaloids

Adam Jozwiak*, Sayantan Panda, Ryota Akiyama, Ayano Yoneda, Naoyuki Umemoto, Kazuki Saito, Shuhei Yasumoto, Toshiya Muranaka, Sachin A. Gharat, Yana Kazachkova, Yonghui Dong, Shlomy Arava, Inna Goliand, Reinat Nevo, Ilana Rogachev, Sagit Meir, Masaharu Mizutani, Asaph Aharoni*

INTRODUCTION: The spatial and temporal organization of molecules is essential for orchestrating cellular metabolism because it allows for the efficient functioning of interconnected biochemical pathways. Metabolite synthesis often requires precise regulation through enzyme assemblies called metabolons, which enhance catalytic efficiency and regulate pathway flux. These complexes facilitate local substrate concentration, prevent side reactions, and protect cells from toxic intermediates. Although primary and secondary metabolic processes in plants likely rely on such enzyme assemblies, direct evidence for complex formation, particularly in those enabling substrate channeling, remains limited. Steroidal glycoalkaloids (SGAs), potent protective compounds in plants, are derived from cholesterol as the main precursor. Cholesterol is transformed through a cascade of complex reactions, yielding a multitude of structurally diverse metabolites, including well-known antinutritional compounds, such as potato alkaloids. A crucial question pertinent to many secondary metabolic pathways—extending beyond plants—is how these pathways intersect with core metabolic processes while minimizing any negative effects on overall fitness. Enzyme mappings in SGA biosynthesis reveal insights into plant strategies that sustain vitality under high demands for secondary metabolites.

RATIONALE: Dietary Solanaceae species, including tomato and potato, produce SGAs critical to their chemical defense. Although past studies have identified more than a dozen enzymes involved in these pathways, a comprehensive picture of SGA biosynthesis is still lacking, which presents a barrier to engineering SGAs in other hosts. Additionally, the mechanisms that coordinate the production of steroidal secondary metabolites with the constitutive accumulation of phytosterols—membrane-embedded lipids closely related to cholesterol—are still unclear. This study identifies GLYCO-ALKALOID METABOLISM15 (GAME15) as the so-called missing link in SGA biosynthesis. GAME15 is proposed to function as both a glucuronosyltransferase enzyme and a scaffold protein within the biosynthetic pathway, coordinating sterol metabolism and enabling the full reconstitution of SGA biosynthesis in various systems.

RESULTS: We discovered that GAME15, a cellulose synthase–like M protein, is localized in the endoplasmic reticulum (ER) and associated with the SGA metabolic gene cluster. GAME15 catalyzes the glucuronidation of cholesterol to produce cholesterol glucuronide and serves as a scaffold to other enzymes involved in SGA biosynthesis. Functional assays conducted in *Nicotiana benthamiana* and yeast demonstrated that GAME15 is critical for directing metabolite flow and facilitating the efficient conversion of cholesterol to SGAs. Silencing *GAME15* in tomato and potato resulted in cholesterol accumulation and a significant decrease in SGA levels, underscoring its essential role in the biosynthesis of SGAs. Protein interaction studies further revealed that GAME15 forms an enzyme complex with other biosynthetic enzymes, enhancing the transfer of intermediates along the pathway for greater metabolic efficiency.

CONCLUSION: GAME15 is essential for the biosynthesis of SGAs in Solanaceae plants, acting as both a glucuronosyltransferase and a scaffold protein that organizes enzyme complexes for efficient metabolic flux. The discovery of GAME15's role in glucuronidation and its function as part of an enzyme assembly complex offers valuable insights into the evolution of complex biosynthetic pathways in plants. This knowledge presents opportunities for engineering SGA biosynthetic pathways in alternative systems, with promising applications across the food, cosmetics, and pharmaceutical industries. ∎

Evolutionary rewiring of GAME15 anchors SGA biosynthesis to the ER for enhanced plant defense.
Schematic of SGA biosynthesis in *Solanum* plants, highlighting GAME15's role in the ER as a bifunctional protein with enzymatic and structural functions that coordinate SGA production. Evolutionary adaptations localize GAME15 to the ER for efficient metabolite production, with implications for engineering, plant defense, pharmaceuticals, and crop antinutritional properties.

READ THE FULL ARTICLE AT
https://doi.org/10.1126/science.adq5721

EMBARGOED UNTIL 2PM U.S. EASTERN TIME ON THE THURSDAY BEFORE THIS DATE:

RESEARCH ARTICLE

PLANT SCIENCE

A cellulose synthase–like protein governs the biosynthesis of *Solanum* alkaloids

Adam Jozwiak[1,2]*, Sayantan Panda[1,3], Ryota Akiyama[4], Ayano Yoneda[4], Naoyuki Umemoto[5], Kazuki Saito[5], Shuhei Yasumoto[6], Toshiya Muranaka[6], Sachin A. Gharat[1], Yana Kazachkova[1], Yonghui Dong[1], Shlomy Arava[1], Inna Goliand[1], Reinat Nevo[1], Ilana Rogachev[1], Sagit Meir[1], Masaharu Mizutani[4], Asaph Aharoni[1]*

Decades of research on the infamous antinutritional steroidal glycoalkaloids (SGAs) in Solanaceae plants have provided deep insights into their metabolism and roles. However, engineering SGAs in heterologous hosts has remained a challenge. We discovered that a protein evolved from the machinery involved in building plant cell walls is the crucial link in the biosynthesis of SGAs. We show that cellulose synthase–like M [GLYCOALKALOID METABOLISM15 (GAME15)] functions both as a cholesterol glucuronosyltransferase and a scaffold protein. Silencing *GAME15* depletes SGAs, which makes plants more vulnerable to pests. Our findings illuminate plant evolutionary adaptations that balance chemical defense and self-toxicity and open possibilities for producing steroidal compounds in heterologous systems for food, cosmetics, and pharmaceuticals.

Spatial and temporal organization of molecules is essential for coordinating metabolism and other numerous actions in a cell. Biosynthesis of certain metabolites requires very strict regulation by formation of enzyme-enzyme assemblies or, in some cases, dynamic metabolons. These allow control over pathway flux by increasing catalytic efficiency. They also enrich local substrates, avoid competing pathways, and protect cells from the accumulation of cytotoxic intermediates (*1*). In some cases, core metabolic processes—such as the tricarboxylic acid (TCA) cycle in yeast and plants; glycolysis in mammals, yeast, and plants; and branched-chain amino acid metabolism in humans—rely on the coordination of multiple protein complexes. Such complexes are thought to facilitate substrate channeling, a crucial aspect of primary metabolism (*2–8*). Additionally, secondary metabolic processes in plants have been reported to involve the organization of metabolons (*9–14*). Nevertheless, only a few studies have proved the formation of assemblies capable of substrate channeling, which is the definitive evidence of metabolon formation (*15*). A scaffold is a distinct, genetically encoded unit that regulates the interaction of enzymatic components, and the development of new scaffold proteins could

provide a simple mechanism for joining preexisting components in unusual new ways (*16*). Scaffold proteins have been found to play a central role in a large number of signaling processes by physically assembling the relevant molecular components (*17*); however, there are only a few examples of their involvement in the regulation of biosynthetic pathways by assembling enzyme complexes. One of the few examples is lignin biosynthesis in *Arabidopsis* that requires involvement of membrane steroid–binding proteins (MSBPs) to physically organize monolignol P450 monooxygenases (*12*). Almost all scaffold proteins most probably work by tying and positioning their partner molecules. Because tethering increases the effective concentration of enzymes and their substrates, it is thought to provide a large entropic benefit (*18*). The ability of scaffold proteins to facilitate the evolution of new pathways is perhaps their most important feature.

Among diverse plant families, Solanaceae species are notable for their ability to produce a wide range of bioactive and toxic metabolites. Among them, antinutritional steroidal glycoalkaloids (SGAs), characteristic of the genus *Solanum*, play an important role in plant defense (*19*). Although the biosynthesis of SGAs is relatively well understood, the functionalities of certain enzymes have never been confirmed, and the reconstitution of an entire biosynthetic pathway has been futile until now. In this work, we report on GLYCOALKALOID METABOLISM15 (GAME15), a missing link in the biosynthesis of *Solanum* SGAs. We discovered that GAME15 is a result of an evolutionary molecular co-opting of the cell wall machinery that encompassed change of subcellular localization

and enzymatic activity. GAME15 evolved as an endoplasmic reticulum (ER) glucuronosyltransferase transferring a glucuronic acid moiety (GlcA) onto cholesterol and serves as a scaffold protein tethering other GAMEs from early steps of the pathway and enabling their functionality. We confirmed that GAME15 links the cholesterol and SGA pathways. The discovery of GAME15 enabled us to engineer the entire eight–enzymatic steps pathway of SGA aglycone biosynthesis in a heterologous plant host.

The SGA gene cluster includes an ER-localized GAME15

Decades of research on SGAs have resulted in major advancements in understanding of their biosynthesis and function. However, despite the large number of functionally characterized biosynthetic genes, it was impossible to engineer the SGA biosynthetic pathway in heterologous hosts. This directed our interest toward finding the missing link that made the reconstitution of the pathway impossible. Genes associated with SGA biosynthesis in tomato and potato are coexpressed; some of them localized to the same genomic region, forming a metabolic gene cluster (Fig. 1, A and C). Clustered genes include *GAME1*, *GAME2*, *GAME6*, *GAME11*, *GAME17*, and *GAME18* from tomato (*19*, *20*) and *StSGT3*, *St16DOX*, *StPGA2*, and *StSGT1* from potato (*21–27*). These SGA clusters included a gene annotated as *cellulose synthase–like M* (*GAME15*), which was highly coexpressed with other *GAME* genes. Apart from *GAME15* presence in a cluster and expression pattern, our previous study demonstrating the involvement of a cellulose synthase–like enzyme in the biosynthesis of glucuronidated triterpenoid saponins had suggested this gene to be involved in the production of tomato SGAs (*28*, *29*). Analysis of the tomato transcriptome in different tissues showed that *GAME15* exhibits a similar expression profile to that of other *GAME*s, especially those involved in early stages of SGA metabolism, and that its expression peaks in green tissues that are especially rich in α-tomatine, the main SGA found in tomato leaves and green fruit (Fig. 1C and fig. S1).

To gain a better understanding of GAME15 function, we performed phylogenetic analysis of cellulose synthase–like enzymes from *Arabidopsis*, different Solanaceae species, and other CesA and CSL proteins (table S1). We discovered that GAME15 from tomato and potato belong to the same clade with other CSL sequences from the nightshade family, and all of them are closely related to the previously characterized SOAP5 from spinach, which catalyzes the attachment of GlcA to the triterpenoid aglycone (*28*) (Fig. 1B). In silico analyses of GAME15 structure and subcellular localization predicted the existence of six transmembrane domains and suggested ER localization (figs. S2 and S3). Confocal

[1]Department of Plant and Environmental Sciences, Weizmann Institute of Science, Rehovot, Israel. [2]Department of Botany and Plant Sciences, University of California, Riverside, CA, USA. [3]Leibniz Institute of Plant Biochemistry, Halle (Saale), Germany. [4]Graduate School of Agricultural Science, Kobe University, Hyogo, Japan. [5]RIKEN Center for Sustainable Resource Science, Yokohama, Kanagawa, Japan. [6]Department of Biotechnology, Graduate School of Engineering, Osaka University, Osaka, Japan.
*Corresponding author. Email: adamj@ucr.edu (A.J.); asaph.aharoni@weizmann.ac.il (A.A.)

Fig. 1. GAME15 is a new player in SGA biosynthesis. (A) SGA metabolic gene clusters in potato and tomato, with genes involved in SGA production marked in color. GAME15 (cellulose synthase–like M) is marked in red and is present in both species. **(B)** Phylogenetic tree of cellulose synthases and cellulose synthase–like proteins from *Arabidopsis*, tomato, and potato. Analysis also included functionally characterized protein sequences from other plant species. Cellulose synthase from the cyanobacteria *Nostoc* was used as an outgroup (see table S1). AA, amino acid; TMD, transmembrane domain. ND indicates not determined. **(C)** Expression pattern of *GAME15* and other *GAME* genes in various tissues of tomato: IG, immature green; MG, mature green; Br, breaker; Or, orange; R, ripe. **(D)** Confocal micrographs showing subcellular localization of GAME15, GAME6, GAME8, and GAME4. Each of the GAME proteins was fused to mRFP (monomeric RFP) and coexpressed with ER marker fused to GFP in *N. benthamiana* leaves. Merge panel shows colocalization of GAME proteins and ER marker. Scale bar, 10 μm. eGFP, enhanced GFP.

microscopy of tobacco leaves expressing tomato GAME15 fused with red fluorescent protein (RFP) showed that it resides in the ER (Fig. 1D) as all the other early-stage SGA biosynthetic enzymes are localized (Fig. 1D). This further supported its possible role in SGA biosynthesis.

GAME15 is a cholesterol glucuronosyltransferase

Because previous work has shown that CSL proteins catalyze glucuronidation of triterpenoid saponins substrates (*28*, *29*), we hypothesized that GAME15 might be an SGA glucuronosyltransferase. However, none of the SGAs detected in tomato thus far contain a GlcA moiety. We therefore decided to examine whether the SGA precursor cholesterol could be glucuronidated by the GAME15 enzyme. To assess this, we transiently expressed *GAME15* in *Nicotiana benthamiana* plants using the *Agrobacterium* infiltration method. Analysis of methanolic

extracts of infiltrated samples showed that in the presence of GAME15, endogenous cholesterol was converted to cholesterol glucuronide (CHR-GlcA) [mass/charge ratio (m/z) = 561.379; Fig. 2A and fig. S4]. We next aimed to determine whether glucuronidation of cholesterol is essential for its downstream metabolism by the GAME6 and GAME8 hydroxylating cytochrome P450 enzymes. We therefore expressed them in *N. benthamiana* leaves with or without the *GAME15* gene. Analysis of cholesterol and its derivatives revealed notable differences between samples containing or lacking GAME15 (Fig. 2, B to D). Tobacco leaves expressing solely GAME6 or GAME8 did not differ from control plants (Fig. 2B). Coexpression of GAME6 with GAME15 produced 22*S*-hydroxycholesterol glucuro-

nide (22-OH-CHR-GlcA) (Fig. 3F), whereas coexpression of GAME8 with GAME15 resulted in the production of 26-hydroxycholesterol glucuronide (Fig. 2B). Simultaneous expression of GAME8, GAME6, and GAME15 in *N. benthamiana* efficiently produced 22,26-dihydroxycholesterol glucuronide (22,26-diOH-CHR-GlcA) (Fig. 2C). Addition of the GAME11, oxoglutarate-dependent dioxygenases (2-ODD) led to the production of trihydroxycholesterol glucuronide (Fig. 2D). To confirm that the observed metabolite is a derivative of cholesterol, we used cholesterol-*d7* (labeled with seven atoms of deuterium) as a substrate, which we coinfiltrated into *N. benthamiana* leaves. Using liquid chromatography–mass spectrometry (LC-MS), we observed incorpora-

tion of the labeled substrate and the production of cholesterol-*d7* glucuronide (m/z = 568.4230; Fig. 2, E and F, and fig. S5). We next confirmed the regio- and stereospecificity of GAME6 and GAME8 by hydrolyzing (removal of sugar moieties) the previously analyzed extracts obtained from plants coexpressing GAME6, GAME8, and GAME15 and reanalyzing them on LC-MS with appropriate standards (22*R*-, 22*S*-, and 26-hydroxycholesterols; fig. S6). This proved that GAME6 produces solely 22*S*-hydroxycholesterol glucuronide, whereas GAME8 hydroxylates cholesterol in position C26.

To corroborate our findings in planta we further tested the activity of GAME15 in yeast cells. Because yeast do not produce UDP-GlcA, which is a substrate for GAME15, we coexpressed
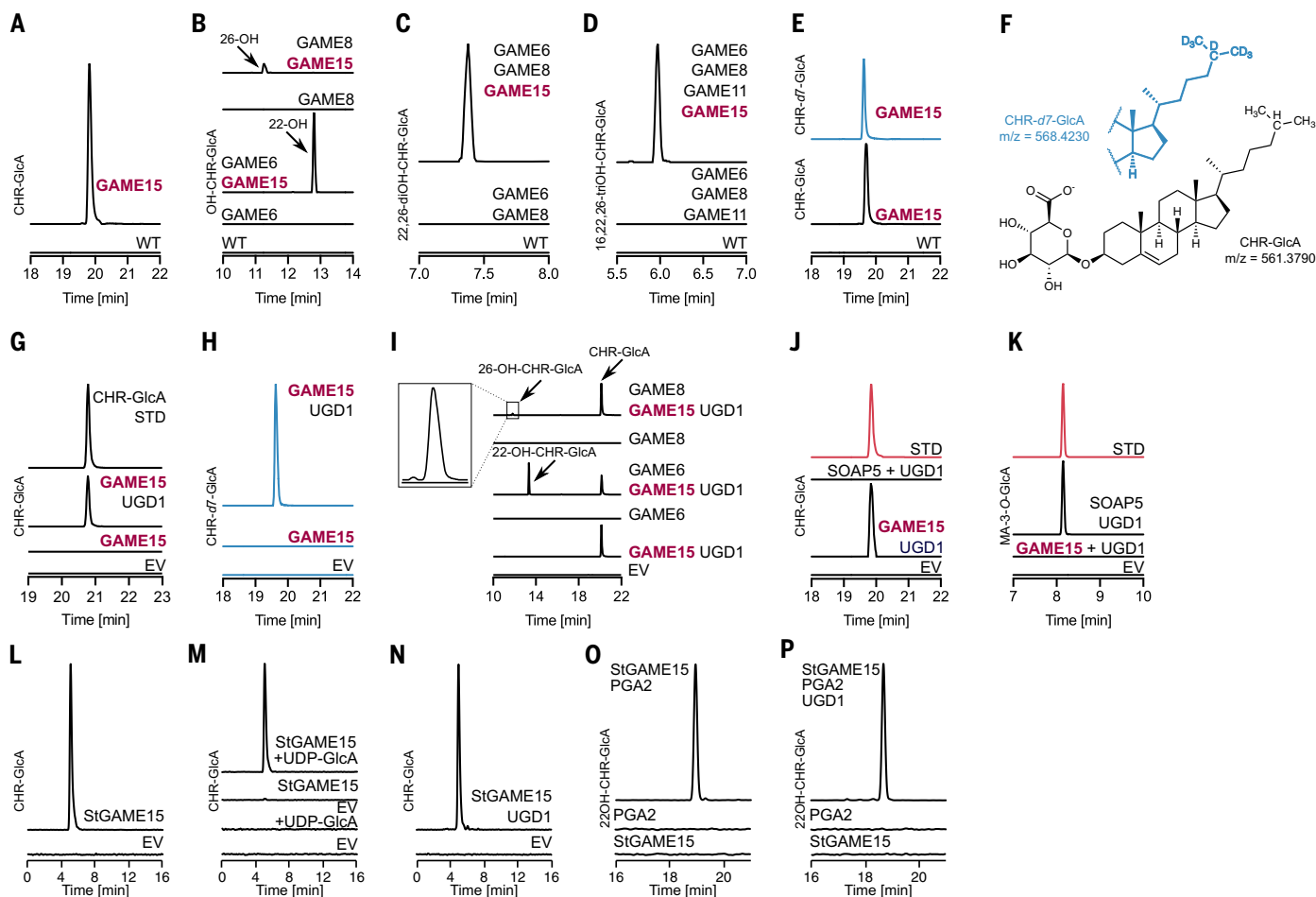
Fig. 2. GAME15 is an active glucuronosyltransferase in planta and in yeast cells. (A to D) LC-MS analysis of *N. benthamiana* leaves expressing GAME15 [extracted ion chromatogram (EIC) m/z 561.379, [M-H]⁻ of CHR-GlcA] (A); GAME6 or GAME8 together with GAME15 (EIC m/z 577.375, [M-H]⁻ of OH-CHR-GlcA) (B); GAME6, GAME8, and GAME15 (EIC m/z 593.369, [M-H]⁻ of diOH-CHR-GlcA) (C); or GAME6, GAME8, GAME11, and GAME15 (EIC m/z 609.364, [M-H]⁻ of triOH-CHR-GlcA) (D). **(E)** Production of CHR-*d7*-GlcA from cholesterol-*d7* in leaves expressing GAME15 [black trace, CHR-GlcA (EIC m/z 561.379); blue trace, CHR-*d7*-GlcA (EIC m/z 568.423)]. **(F)** Structures of CHR-GlcA and CHR-*d7*-GlcA with deuterium atoms indicated. **(G)** LC-MS analysis of cholesterol-supplemented

yeast cells expressing GAME15 and UGD1 (EIC m/z 561.379 of CHR-GlcA). **(H)** Production of CHR-*d7*-GlcA from cholesterol-*d7* in yeast expressing GAME15 (EIC m/z 568.423). **(I)** LC-MS of yeast cells expressing GAME15, UGD1, GAME6, or GAME8 (EIC for m/z 561.379 and 577.375). **(J and K)** LC-MS of yeast expressing GAME15+UGD1 or SOAP5+UGD1 fed either with cholesterol (EIC m/z 561.379) (J) or medicagenic acid (EIC m/z 677.354) (K). **(L to P)** LC-MS/MS analysis of insect cells expressing StGAME15 (L), an in vitro assay product using recombinant StGAME15 prepared with insect cell (M), yeast expressing StGAME15 and UGD (N), insect cells expressing StGAME15 and PGA2 or StGAME6 (O), and yeast expressing StGAME15 and PGA2 (P).
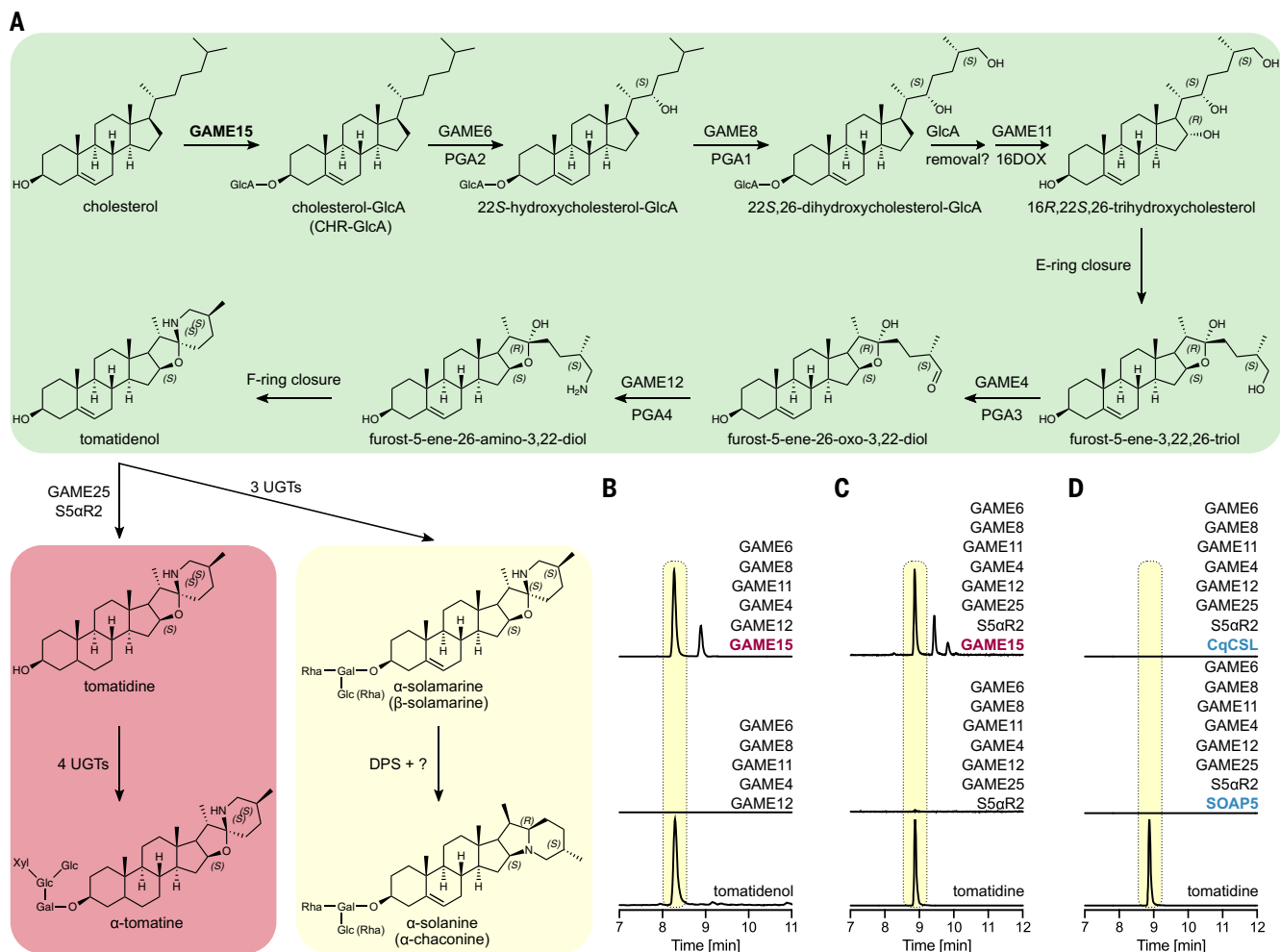
Fig. 3. GAME15 is key for SGA production and engineering in heterologous hosts. (**A**) Updated SGA biosynthetic pathway, including steps with GAME15, GAME6, and GAME8. (**B** to **D**) LC-MS analysis of *N. benthamiana* leaves transiently expressing GAME6, GAME8, GAME11, GAME4, and GAME12 with GAME15 (EIC of *m/z* 414.337) (B); GAME6, GAME8, GAME11, GAME4, GAME12, and GAME25 S5αR2 with GAME15 (EIC of *m/z* 416.352) (C); and GAME6, GAME8, GAME11, GAME4, and GAME12 with SOAP5 or CqCSL instead of GAME15 (EIC of *m/z* 416.352) (D).

GAME15 with UGD1 (UDP-GLUCOSE DEHYDROGENASE 1 from spinach) converting UDP-Glc to UDP-GlcA. Merely simultaneous expression of GAME15 and UGD1 led to the production of CHR-GlcA in yeast cells (Fig. 2G). To confirm the nature of the observed metabolite, we used cholesterol-*d*7 and observed that it was efficiently converted to cholesterol-*d*7 glucuronide in yeast cells only in the presence of GAME15 and UGD1 (Fig. 2, F and H). Further conversion of CHR-GlcA by GAME6 and GAME8 was also possible in yeast cells (Fig. 2I). To test whether GAME15 and SOAP5 have overlapping substrate specificity and whether GAME15 can attach GlcA to medicagenic acid or SOAP5 can glucuronidate cholesterol, we expressed the respective enzymes in yeast cells (together with UGD1) and fed them with either cholesterol or medicagenic acid. LC-MS analysis showed that SOAP5 is very specific toward triterpenoid medicagenic acid and cannot modify choles-

terol. Similarly, GAME15 was only able to attach GlcA to cholesterol (Fig. 2, J and K).

Further experiments showed that GAME15 expressed in yeast cells could not only accept cholesterol as a substrate but also other sterols, including ergosterol, episterol, zymosterol, fecosterol, and even lanosterol (fig. S7). By contrast, GAME15 expressed in planta (i.e., *N. benthamiana*) was able to attach GlcA only to cholesterol, and we could not detect other glucuronidated sterols (e.g., *beta*-sitosterol, stigmasterol) (fig. S8). We next investigated whether stigmasterol-GlcA or sitosterol-GlcA, potential products of GAME15 activity, were further modified by *N. benthamiana* enzymes. However, we were unable to detect any metabolites derived from these two sterols. Additionally, we hypothesized that GAME15 enzyme specificity might be restricted to C27 (cholesterol) and C28 (fecosterol, ergosterol) sterols. To test this, we correlated the amount of

cholesterol and campesterol with their glucuronidated derivatives in *N. benthamiana* leaves expressing the GAME15 protein. Although campesterol levels were three times as high as cholesterol in this tissue, the accumulation of campesterol-GlcA was almost 45-fold lower compared with CHR-GlcA, which indicates that GAME15 exhibits strong specificity for cholesterol in planta (fig. S9). This suggests that GAME15 specificity is determined not by the type of sterol but rather by the protein-protein interactions between cholesterol and SGA biosynthetic enzymes. The aforementioned results suggest that cholesterol glucuronidation by GAME15 is essential for the conversion of cholesterol to tomatidine in the SGA biosynthetic pathway.

Next, we performed functional analysis of potato GAME15. We expressed the potato GAME15 in insect cells, which produce cholesterol as a main sterol. Analysis of the insect

cell extracts confirmed the production of CHR-GlcA upon expression of potato GAME15 (Fig. 2L). In vitro assays using microsomal fractions of the insect cells, with cholesterol as a substrate, demonstrated the formation of CHR-GlcA in the presence of UDP-GlcA (Fig. 2M). Similarly, coexpression of potato GAME15 and UGD1 in cholesterol-producing yeast also confirmed the production of CHR-GlcA (Fig. 2N). Furthermore, coexpression of PGA2 (StGAME6) with potato GAME15 resulted in the production of 22-hydroxycholesterol-GlcA in both insect cells and yeast (Fig. 2, O and P).

GAME15 orchestrates biosynthesis of SGAs and enables engineering

Attempts to reconstitute the biosynthetic pathway of SGAs in heterologous hosts, such as yeast or plants, had failed so far. We therefore examined whether GAME15 could be the missing factor in engineering SGAs. At first, we infiltrated tobacco leaves with *GAME6* (cholesterol C22 hydroxylase), *GAME8* (C26 hydroxylase), *GAME11* (C16 hydroxylase), *GAME4* (C26 oxidase), or *GAME12* (aminotransferase), with or without *GAME25* and *5-alpha-reductase* (performing C5 double bond reduction) (Fig. 3A). This set of genes should facilitate the conversion of cholesterol to tomatidine; however, we did not detect the formation of any product in planta (Fig. 3, B and C). Notably, expressing the same combination of genes together with *GAME15* resulted in efficient production of tomatidenol or tomatidine in tobacco leaves (Fig. 3, B and C). We also checked whether SOAP5 (CslM from spinach) or CqCSL from quinoa (*Chenopodium quinoa*) can substitute for GAME15 in engineering SGA biosynthesis in *N. benthamiana* leaves. Transient expression of SOAP5 or CqCSL, together with tomato GAME genes, did not facilitate the production of tomatidine (Fig. 3C). Additionally, the fact that transient expression experiments in *N. benthamiana* (Solanaceae) without GAME15 did not yield tomatidine indicates that the endogenous NbCSL enzyme, closely related to the tomato one (75% identity, median split 23.9 million years ago), does not serve the same function or it is not expressed at all. Furthermore, we inferred that GAME15 gain of function was a recent evolutionary event and is likely restricted to species from the *Solanum* genus (fig. S9).

GAME15-silenced plants lack CHR-GlcA and SGAs

We next generated tomato and potato *GAME15* RNA interference (*GAME15i*) lines (fig. S10). Metabolite analysis of the RNAi tomato leaves showed a notable reduction in SGA content, with α-tomatine levels reduced on average by 35-fold as compared with wild type (WT) (Fig. 4A). We observed the same phenomenon in potato RNAi lines in which *GAME15* silencing

resulted in a marked reduction in α-solanine and α-chaconine accumulation (Fig. 4, K and L). On the other hand, LC-MS and gas chromatography–mass spectrometry (GC-MS) analysis of sterols showed high accumulation of cholesterol and cholesteryl glucoside in the *GAME15i* tomato and potato lines (Fig. 4, B, C, M, and N, and fig. S11). Additionally, silencing *GAME15* resulted in the complete depletion of CHR-GlcA in tomato leaves (Fig. 4D). We used matrix-assisted laser desorption/ionization–mass spectrometry imaging (MALDI-MSI) to monitor the spatial distribution of α-tomatine and cholesterol in WT and *GAME15i* tomato fruit at two developmental stages (Fig. 4E). Spatial metabolite analysis was also carried out for the major potato SGAs (α-chaconine and α-solanine) in WT and *GAME15i* tubers (Fig. 4J). We observed that in WT green and breaker tomato fruit, α-tomatine was highly abundant in the skin, whereas it was completely depleted from *GAME15i* fruit (Fig. 4E). MALDI-MSI also showed marked accumulation of cholesterol in all stages of tomato fruit development (Fig. 4E). Similarly, in potato, the α-chaconine and α-solanine SGAs were undetectable, whereas cholesterol levels surged in *GAME15i* tubers' outer layers (Fig. 4J).

We next used virus-induced gene silencing (VIGS) in *Solanum pennellii* to examine the effect of reduced expression of *GAME6*, *GAME8*, and *GAME11* genes on the accumulation of SGAs and their intermediates. Silencing each one of the three genes resulted in a reduced accumulation of α-tomatine and dehydrotomatine (fig. S12). We also observed that silencing *GAME6* resulted in an increased accumulation of CHR-GlcA, the immediate precursor for this enzyme (Fig. 4F). Silencing *GAME8*, on the other hand, affected the conversion of 22-hydroxycholesterol-GlcA to dihydroxycholesterol-GlcA (Fig. 4G). Notably, silencing *GAME11* did not lead to an increased accumulation of dihydroxycholesterol-GlcA but rather dihydroxycholesterol hexoses (Fig. 4, H and I, and fig. S13), which supports the hypothesis that the GlcA moiety is removed by an unknown glycosidase once CHR-GlcA is hydroxylated at positions C22 and C26 (Fig. 3A). However, as mentioned before, in *N. benthamiana* expressing GAME6, GAME8, GAME11, and GAME15, we could detect trihydroxycholesterol glucuronide, which suggests that GAME11 can also accept glucuronidated substrate.

We also analyzed SGA pathway metabolites in various mutants of potato plants deficient in key SGA biosynthetic genes. In *GAME15* knockout potato hairy roots, CHR-GlcA was not detected (Fig. 4O). *PGA2* (*StGAME6*) RNA interference (*PGA2i*) potato plants exhibited higher levels of CHR-GlcA compared with non-transgenic potato plants (Fig. 4P). In *PGA1* (*StGAME8*)–knockout potato hairy roots, the accumulation of 22-hydroxycholesterol-GlcA was confirmed (Fig. 4Q).

Monocot cholesterol hydroxylating enzymes do not require GAME15 activity

Considering the involvement of cytochrome P450s in the biosynthesis of verazine, a steroidal alkaloid from *Veratrum californicum* (30), and diosgenin from monocot species (i.e., *Paris pollyphyla* and *Dioscorea zingiberensis*) (31, 32), we investigated whether GAME15 dependency for cholesterol hydroxylation and further conversion into SGAs is *Solanum* specific or occurs in other taxa as well. We used CYP90B95 (C22 hydroxylation, GAME6 equivalent), CYP90G8 (C16,22 hydroxylation, GAME11 equivalent), and CYP94D181 (C26 hydroxylation, GAME8 equivalent) from the monocot species *Liriope muscari* (Asparagaceae) for experiments in tobacco plants. Expression of the *Liriope* CYPs in tobacco led to the production of diosgenin (fig. S14); the addition of GAME4 and GAME12 resulted in the production of solasodine (25R-tomatidenol) (fig. S15). This led us to conclude that the production of SGAs by the *Liriope* CYPs is GAME15 independent, and GAME4 and GAME12 do not require GAME15 (Fig. 3G). On the basis of our results from *GAME11* silencing experiment in *S. pennellii* and the literature, we assumed that GAME11 is also GAME15 independent because it could accept 22,26-dihydroxycholesterol without a GlcA moiety (22).

GAME15 participates in cholesterol-SGA biosynthetic assembly

The high in planta substrate specificity of GAME15 toward cholesterol, which is not observed in yeast cells where GAME15 can glucuronidate not only cholesterol but also other sterols, suggested that GAME15 might have an additional role in the SGA pathway and not merely cholesterol glucuronosyltransferase activity. We hypothesized that such an additional function could be as an ER-localized scaffold protein facilitating the formation of a protein complex. If this is confirmed, SGAs biosynthesis is likely to be carried out in the form of a metabolon in which metabolite channeling occurs between consecutive pathway enzymes. To test this theory, we conducted a series of experiments, the first being the study of tomato GAME15 interaction with the cholesterol and SGA pathway enzymes. We used in planta fluorescence lifetime imaging microscopy–Förster resonance energy transfer (FLIM-FRET) to test protein proximity. The FLIM-FRET method is based on the measurement of a FRET donor lifetime (in this case, GAME15-GFP), which decreases when FRET occurs between the donor and an acceptor (in this case, another protein fused to RFP; fig. S16). We measured lifetimes for multiple pairs and observed a significant reduction in the donor's lifetime while coupling with GAME6, GAME8, and the cholesterol biosynthesis proteins 7-DR2 (7-DEHYDROCHOLESTEROL REDUCTASE 2)
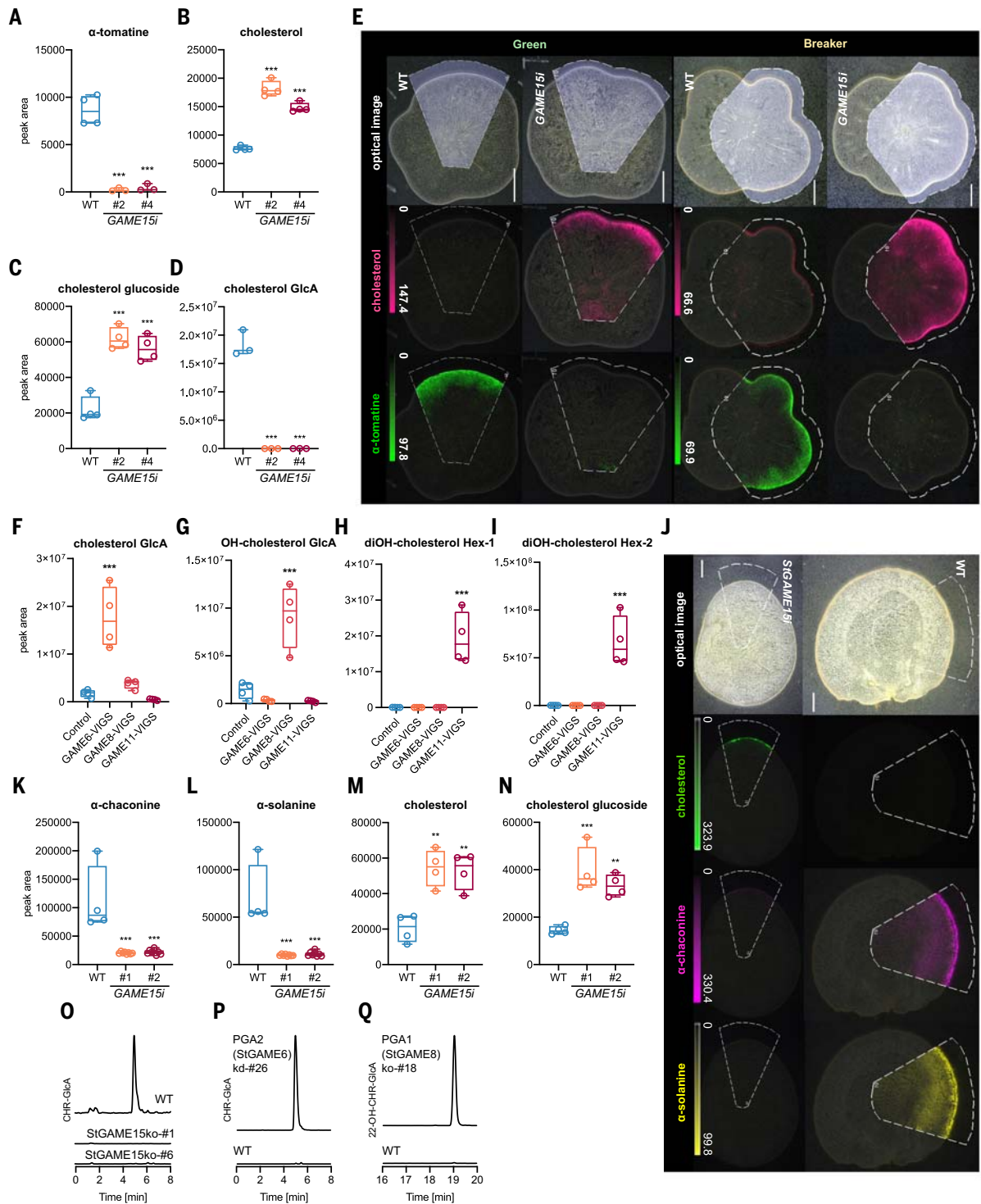
Fig. 4. Silencing of *GAME15* in tomato and potato leads to cholesterol accumulation. (**A** to **C**) LC-MS analysis of *SlGAME15i* lines showing levels of α-tomatine (A), cholesterol (B), and cholesterol glucoside (C). (**D**) CHR-GlcA levels in *GAME15i* lines. (**E**) MALDI-MSI of WT and *GAME15i* tomato fruit at immature green and breaker stage. Upper, middle, and lower panels show optical images of analyzed specimen, distribution of cholesterol, and distribution of α-tomatine in the fruit, respectively. (**F** to **I**) VIGS of *GAME6*, *GAME8*, or *GAME11* genes in *S. pennellii* led to increased accumulation of CHR-GlcA (F), OH-CHR-GlcA (G), and two isomers of diOH-cholesterol glycosides [(H) and (I)]. (**J**) MALDI-MSI of WT and *GAME15i* potato tubers. Upper panels show optical

images of analyzed specimens, second-row panels show distribution of cholesterol, and the bottom panels show the distribution of α-chaconine and α-solanine. (**K** to **N**) LC-MS analysis of α-chaconine (K), α-solanine (L), elevated levels of cholesterol (M), and cholesterol glucoside (N) in potato *GAME15i* lines. (**O**) LC-MS/MS analysis of *StGAME15-ko* potato hairy root. MRM chromatogram of *m/z* 596 > 385 is shown. (**P**) LC-MS/MS analysis of *PGA2/StGAME6i* potato. (**Q**) LC-MS/MS analysis of *PGA1/StGAME8ko* potato hairy roots. Asterisks indicate significant differences determined by Student's *t* test (**P* < 0.01; ****P* < 0.001). Box plots show median values as bars, with error bars representing minimum and maximum values. All individual data points are shown (*N*).

and C5-SD2 [STEROL C-5(6) DESATURASE 2] (fig. S17) (*33*). This reduction in lifetime could be translated to a FRET efficiency (Fig. 5A), confirming their proximity to GAME15 (Fig. 5). We did not observe interaction with GAME4, GAME7, or GAME11. In these FLIM-FRET measurements, we used green fluorescent protein (GFP) fused to RFP as a positive control (FRET efficiency, 23.5%; fig. S17). We also used multiple negative controls: GFP and RFP (FRET efficiency, 1.9%), GAME15-GFP + SOAP4-RFP (P450 from spinach involved in triterpenoid saponin biosynthesis; FRET efficiency, 4.5%), and GAME15-GFP + F5H-RFP (P450 with ferulate-5-hydroxylase activity; FRET efficiency, 3.3%), all showing <5% FRET efficiency, which was used here as a limit for protein-protein interaction (*10*). Notably, the CYP protein C4H (cinnamate-4-hydroxylase), involved in the same biosynthetic pathway as F5H and proven to form an enzyme-enzyme complex with it and other flavonoid biosynthetic enzymes, did show strong FRET with GAME15 (efficiency at 11.1%). This could be explained by the fact that P450s GAME6 and GAME8, as well as C4H, require the presence of cytochrome P450 reductase (POR) that might be common for these cytochromes and thus be located in close proximity to GAME15. The same results were obtained in tandem affinity purification–mass spectrometry (TAP-MS) and in planta split luciferase complementation assay experiments described below.

In TAP-MS assays, expression of GFP-tagged GAME15 and other GAME enzymes (i.e., GAME6, GAME8, GAME4, GAME11, GAME12, and GAME25) and cholesterol biosynthesis proteins (i.e., C5-SD2 and 7-DR2) in *N. benthamiana* and subsequent liquid chromatography–tandem mass spectrometry (LC-MS/MS) analysis of affinity-purified proteins confirmed the FLIM-FRET results. In this experiment, we detected 314 proteins with at least two peptides. After filtering, we obtained a list containing 114 proteins that were copurified during the immunoprecipitation (IP) process (table S2). Only in a sample expressing GAME15-GFP could we detect GAME6, GAME8, 7-DR2, and C5-SD2 (Fig. 5, B and C). Affinity-purified samples from plants expressing (i) GFP only; (ii) GFP and GAMEs (GAME6, GAME8, GAME4, GAME11, GAME12, and GAME25) together with C5-SD2 and 7-DR2; or (iii) only GAMEs, C5-SD2, and 7-DR2 did not contain any of the mentioned SGA-related proteins (Fig. 5, B and C). Additionally, only in samples expressing GAME15-GFP did we detect endogenous C4H and other CYPs, POR, cytochrome b5, proteins involved in the insertion of polytopic transmembrane proteins into the ER [protein transport protein Sec61 subunit alpha, signal recognition particle (SRP), and ER membrane protein complex (EMC)], as well as dolichyl-diphosphooligosaccharide transferase (DDOST), a glycosyltransferase in-

volved in protein glycosylation (fig. S18). This suggests that during affinity purification, we may not only be purifying GAME15-GFP and its interacting proteins but also microsomes that formed during tissue lysis. To address this possibility, we performed proteomic analysis on both the crude cell lysate and the purified protein fraction after affinity purification. The results showed a significant increase in the relative abundance of GAME enzymes, whereas the concentrations of other proteins decreased during the purification process, which confirms that the purified proteins are part of an enzymatic complex (fig. S19). However, proteins such as Sec6 and DDOST could be contaminants, which are notoriously difficult to avoid in affinity purification methods.

In planta split luciferase complementation assays confirmed the close proximity of GAME15 with GAME6, GAME8, C5-SD2, and 7-DR2 (Fig. 5D). We also observed that GAME4 and GAME11 could complement split luciferase with GAME15 in this assay. Because we did not detect these interactions in previous assays, it may suggest that it is either a false positive interaction or that the split luciferase assay is capable of detecting the proximity of more distant or weakly associated proteins that could be too far to generate efficient FRET or to be dissociated during extensive washes in the affinity purification assay. The findings from multiple assays, as described above, strongly support that GAME15 is a part of a complex comprising cholesterol and SGA biosynthetic proteins, and that it plays a role as the scaffold allowing the conversion of cholesterol to SGAs.

GAME15 facilitates the flow of intermediates in the SGA pathway

The discovery of GAME15 interaction with other proteins and its definite importance to SGA biosynthesis spurred us to examine whether GAME15 acts as a scaffold protein of a metabolon generating SGAs. To investigate this, we assessed the possibility of metabolite channeling—a process involving metabolon formation—by expressing GAME proteins (GAME6, GAME8, GAME11, GAME4, GAME12, and GAME15) in *N. benthamiana* and applying the labeled intermediate $[^2H_6]$cholesterol (cholesterol-*d6*). Metabolon formation could create a closed environment, restricting the diffusion of frequently toxic intermediates while hindering the incorporation of externally applied ones. We followed the incorporation of deuterium-labeled cholesterol into SGAs by measuring labeled and unlabeled products (Fig. 5, E to H). As a control, we used a set of monocot enzymes that are GAME15 independent and do not require metabolon formation for their activity (fig. S15). Our results showed relatively low label incorporation with the GAME enzymes, as merely 0.5% of the detected tomatidenol originated from labeled cholesterol, whereas

in the case of the *Liriope* enzymes, the incorporation of the labeled intermediate was about 20 times as high ($P = 6.218 \times 10^{-11}$) (Fig. 5E). This notable difference suggests metabolite channeling. To rule out the possibility that the *Liriope* monocot enzymes are poorly expressed compared with GAMEs, which could affect enzyme kinetics, cosubstrate availability, and ultimately levels of metabolites detected in our assays, we conducted additional experiments correlating protein expression levels with metabolite production in *N. benthamiana*. We observed that enzymes from *Liriope* were expressed at comparable levels to GAMEs (fig. S20). Still, production of SGA aglycones was approximately two- to threefold higher in plants expressing monocot enzymes (fig. S20). However, this difference does not seem to account for the much higher incorporation of labeled cholesterol in the case of the *Liriope* enzymes, and it supports increased metabolite flux because GAME enzymes possibly mediate channeling.

GAME15 drives SGA production and plant defense

We also generated CRISPR-Cas9 *StGAME15-ko* potato plants (*Solanum tuberosum* cv. Desirée) and obtained three independent *CSL* edited lines (no. 3, no. 8, and no. 11; fig. S21) that showed significant reduction in alkaloid (α-solanine and α-chaconine) production (Fig. 6A). We used these *StGAME15-ko* plants to study their susceptibility to insect infestation that would potentially confirm insecticidal properties of SGAs. In insect choice assay, we exposed WT and *StGAME15* edited plants to highly polyphagous larvae of *Spodoptera littoralis*. After 48 hours, we observed that *St*GAME15 edited plants lacking SGAs were significantly preferred by insects compared with WT, visualized by measuring leaf area consumed by the larvae (Fig. 6, B and C). Additionally, we used no-choice insect assay to see how SGA affects insect growth. The weight of *S. littoralis* fed with leaves from *StGAME15-ko* plants was significantly higher ($P < 0.01$; Student's *t* test) as compared with the weight of those fed with WT plants (Fig. 6D). Thus, removal of SGAs by knocking out *GAME15* in tomato leads to plant hypersusceptibility to pests.

Discussion

Plants and fungi produce numerous secondary metabolites that play key roles in their development and regulate interactions with both allies and adversaries, tailored to their ecological functions. These structurally diverse metabolites exhibit both harmful and beneficial effects not only to humankind but even more so to the organism itself. SGAs, for example, are renowned antinutritional factors for humans while being potent defense agents for plants and simultaneously self-toxic at a certain threshold. How do plants balance the need for highly
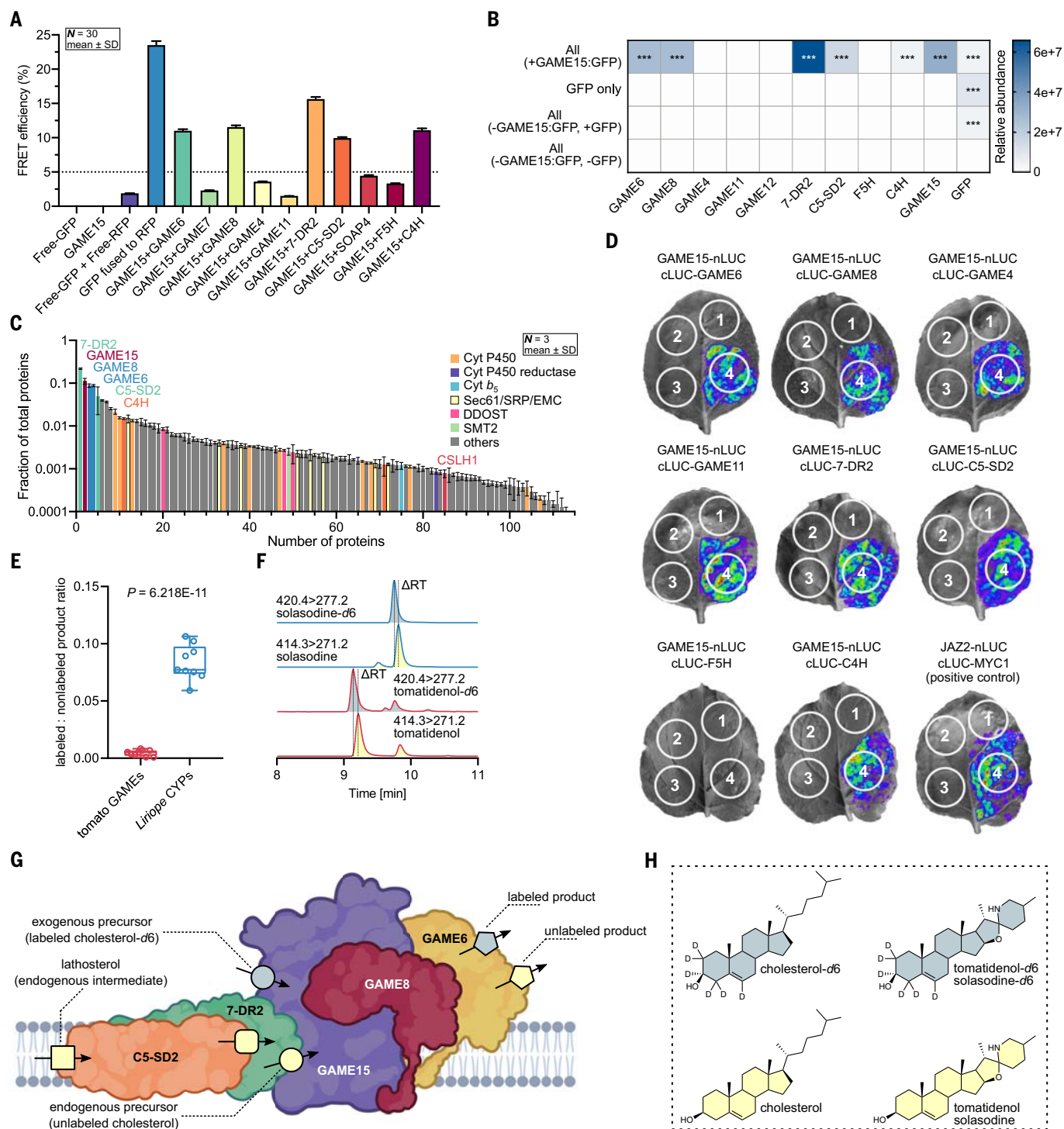
Fig. 5. GAME15 interacts with other GAMEs and facilitates channeling of intermediates. (**A**) Protein interactions among SGA pathway enzymes in *N. benthamiana* were analyzed using FLIM with GAME15 labeled with eGFP and other GAMEs labeled with mRFP1. FRET percentages, indicating protein proximity, were derived from eGFP lifetime measurements (fig. S15), with error bars showing standard deviation (±SD). (**B**) Protein abundance from TAP-MS analysis (***$P < 0.001$; Student's *t* test). (**C**) MS analysis of affinity-purified GAME15-GFP associated proteins, highlighting SGA biosynthesis-related enzymes. Data are shown as fractions of total protein content, with mean values and standard deviations (±SD) from three independent measurements; the ordinate axis is in $\log_{10}$ scale. (**D**) Split luciferase assays to confirm interactions between GAME15 and other GAMEs. GAME15-nLUC was coinfiltrated with cLUC fusions of various proteins. Infiltration combinations are numbered: (1) cLUC-EV+nLUC-EV; (2) GAME15-nLUC; (3) nLUC-EV+cLUC+other protein; and (4) GAME15-nLUC+cLUC-GAMEs. Images were taken 48 hours postinfiltration in *N. benthamiana* leaves, with positive and negative controls included. (**E**) Metabolic channeling using cholesterol-*d*6 to assess exogenous cholesterol incorporation into SGAs in *N. benthamiana*. The graph shows the ratio of labeled to nonlabeled product, reflecting channeling efficiency. (**F**) LC-TQ-MS analysis of labeled and nonlabeled tomatidenol and solasodine, highlighting isotope effects. (**G**) Diagram of metabolite channeling concept. (**H**) Chemical structures of precursors and products used in the channeling experiment. Box plots show median values as bars, with error bars representing minimum and maximum values. All individual data points are shown (*N*).

Fig. 6. Knockout of *GAME15* in potato plants leads to increased susceptibility to insects. (**A**) Relative levels of α-solanine and α-chaconine in WT and *StGAME15-ko* potato plants, showing complete reduction of SGAs in *StGAME15*-edited plants. n.d., not detected.
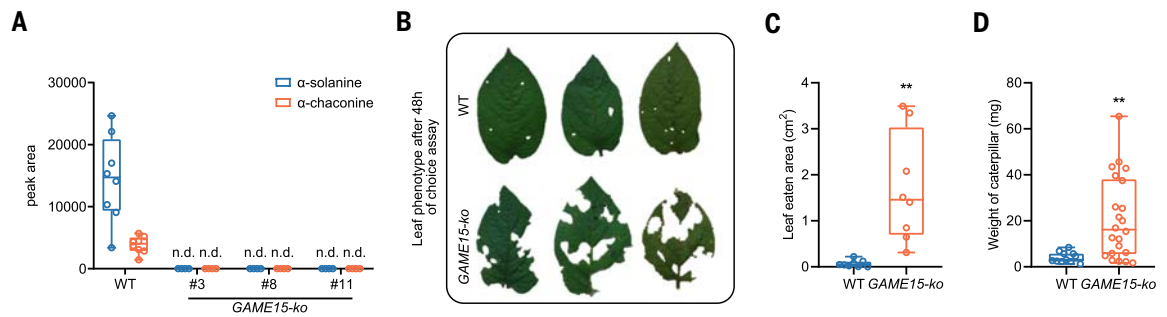
(**B**) Leaf phenotype of the *StGAME15-ko* and WT potato plants after 48 hours of *S. littoralis* insect choice assay. (**C**) Quantification of leaf area eaten by *S. littoralis* larvae in the choice assay after 24 hours. Leaf area is represented in square centimeters. (**D**) Growth assay showing increased weight of caterpillars fed on *StGAME15-ko* lines compared with WT tomato leaves. Asterisks indicate statistically significant differences as compared with WT determined by Student's *t* test (*P < 0.01). Box plots show median values as bars, with error bars representing minimum and maximum values. All individual data points are shown (*N*).

potent defense metabolites and, at the same time, protect themselves from the toxicity of these molecules to their own cells? Our discoveries provide a mechanism in which self-toxicity is prevented through glucuronidation of the secondary metabolite precursor (i.e., cholesterol) rather than typically observed by glycosylating pathway end products.

Several studies have shown that in the case of SGAs, pathway intermediates are highly self-toxic to tomato plants. Previous work (*20*) down-regulated *GAME1* galactosylating tomatidine (the α-tomatine aglycone) and found that it is highly auto-toxic and that its accumulation results in severe plant growth phenotypes. Similar self-toxicity phenotypes were observed a decade later by Kazachkova *et al.* (*34*), who showed that SGAs' sequestration to the vacuole is a self-protection mechanism. Overexpression of the α-tomatine vacuolar exporter GORKY results in the accumulation of SGA pathway intermediates in the cytosol, causing severe plant symptoms. Silencing *GAME15* in three *Solanum* species—i.e., potato, eggplant, and tomato (the latter discussed in this work)—resulted in sharp buildup of cholesterol and a substantial adverse effect on the corresponding plant development and reproduction (fig. S22). These findings implied that the specific attachment of a GlcA moiety to cholesterol by GAME15 is crucial to overcome the damaging consequence of cholesterol accumulation in plant cells.

Results from our study provide an explanation for why cholesterol is initially glucuronidated before its conversion to SGAs in a series of hydroxylations and additional downstream reactions. Phylogenetic analysis revealed that GAME15 CslM-type proteins from both tomato and potato are related to SOAP5 and similar proteins attaching GlcA to the triterpenoid saponins backbone (*28, 29*). However, the evolved GAME15 substrate specificity is restricted exclusively to a set of steroidal metabolites. Activity

with this defined array of substrates likely avoids interference with sterols essential for regulating membrane fluidity and permeability. Furthermore, glucuronidation by GAME15 modifies cholesterol in such a way that it is no longer accessible for hydroxylation by CYP enzymes involved in brassinosteroid biosynthesis, and this consequently prevents the formation of toxic intermediates affecting hormonal balance. Curiously, the first two hydroxylating enzymes GAME6 and GAME8 in the SGA pathway accept merely GlcA decorated and not free cholesterol, and thus SGAs–producing plants avoid the production of potentially self-toxic 22- and 22,26-dihydroxycholesterol (*35*). Additionally, the presence of *GAME15*, *GAME6*, and *GAME11* in one gene cluster may reduce the chances of gene deletion owing to chromosome segregation in crossing.

It is thought provoking that GlcA was specifically selected for cholesterol glycosylation and not an alternative sugar moiety that commonly decorates plant small molecules—e.g., glucose, galactose, xylose, rhamnose, and others (*36*). Even more, no UDP-glucosyltransferase (UGT) or sterol glycosyltransferases (SGTs) reported to glucosylate various tomato sterols, including cholesterol (*37*), evolved to perform the cholesterol glucuronidation reaction. It has also been reported that *Solanum* species accumulate sterols decorated with galactose moiety, which is the first sugar attached to the aglycone in tomato SGAs (*38*). Notably, attachment of galactose to cholesterol instead of GlcA would reduce the number of pathway steps, making it more efficient (*38*).

The enhanced specificity of GAME15 in planta further stems from the formation of a metabolon that involves enzymes from both the cholesterol and SGA biosynthetic pathways. The metabolon component 7-DR2 catalyzes the ultimate reaction to cholesterol, and this ensures direct channeling of the core precursor metabolite for GlcA modification by GAME15

and the subsequent C22 and C26 hydroxylation steps by GAME6 and GAME8, respectively. The presence of cholesterol pathway proteins in the metabolon complex was enabled by the fact that SGAs-producing plants use one set of enzymes for cholesterol and another for phytosterol production (*33*). We postulate that the GAME15 protein evolved in a way to purely interact with cholesterol-producing proteins, hence avoiding the use of other sterols that play crucial roles in maintaining membrane stability.

Attachment of GlcA to the aglycon and its absence in α-tomatine raises the questions of how this sugar is removed and in which cellular compartment hydrolysis occurs. On the basis of the work of Nakayasu *et al.* (*22*) and results presented here, we predict that the GlcA moiety is removed after GAME8 hydroxylation of the C26 position and just before the GAME11 hydroxylation reaction. We suggest that at the ER membrane–cytoplasm interface, a cytosolic or ER-associated glycosidase hydrolyses the GlcA moiety. Once this occurs, GAME11 hydroxylates position C16, and an ER-localized GAME4 CYP further oxidizes the C26 hydroxyl group, facilitating the introduction of nitrogen to the molecule by the GAME12 γ-aminobutyric acid (GABA) transaminase (Fig. 3A and fig. S23). The identity of the GlcA hydrolyzing enzyme and how SGA pathway proteins that are not bona fide ER membrane localized proteins (i.e., the CYPs) associate spatially and physically to the metabolon assembly require further exploration.

The likely GAME15 ancestor protein is cellulose synthase (CesA) that is likewise structured in a complex, albeit in the plasma membrane, and constructs cellulose fibrils. Evolution of GAME15 functions as a cholesterol glycosyltransferase and a core metabolon component gives every indication that its evolvement was explicitly directed for absolute control over cholesterol levels. Particularly in *Solanum* species

making SGAs, cholesterol is a hub metabolite at the primary-secondary metabolism interface; hence, it required the evolution of new mechanisms to avoid undesirable effects to plants.

This study echoes how limited our current knowledge is with respect to mechanisms that govern the biosynthesis of plant secondary metabolites. The evolution of new metabolic pathways and metabolites is dependent on and heavily constrained by the need for an undisruptive solution that sustains core metabolism function with no adverse effects on plant development, defense, and reproduction. As more such mechanisms are discovered with time, our capability to reconstitute these metabolic pathways in heterologous systems and to make desired products will continuously increase. The discovery of GAME15-dependent glucuronidation and its role in forming a metabolon provides a key to engineering SGAs for food, cosmetics, and pharmaceuticals.

Materials and methods
Chemicals

Unless otherwise specified, chemicals used in this study were purchased from Sigma-Aldrich. Standard of CHR-GlcA was from TRC (no. TRC-C174350, Canada).

Plant material

Tomato (*Solanum lycopersicum* cultivar Micro-Tom) and *N. benthamiana* plants were grown in a greenhouse with 24°C:18°C day:night temperatures and a 16-hour:8-hour light:dark photoperiod cycle.

Potato (*S. tuberosum* cultivar Sassy) plants were cultivated 16-hour:8-hour light:dark photoperiod in plant thermostatic chambers at 25°C.

Transgenic CRISPR-Cas9 mutant plants were generated in the potato (*S. tuberosum* cv. Desirée) background.

Generation of transgenic plants

RNA interference construct used to generate *GAME15-RNAi* tomato lines was generated using the Gateway system (*39*).

To generate potato *StGAME15-ko* lines, four guide RNAs (gRNAs) were selected from *StGAME15*, and gRNA expression cassettes were assembled into CRISPR-Cas9 vector as described by Sonawane *et al.* (*40*). The CRISPR-Cas9–gRNA construct was introduced into *Agrobacterium tumefaciens* (GV3101) electrocompetent cells and later transformed into potato (*S. tuberosum* cv. Desirée) leaf explants, as described previously (*41*). Plantlets with roots were transferred to greenhouse for further analysis. CRISPR-Cas9–induced mutations were genotyped in T0 plants using DNA sequencing as described by Sonawane *et al.* (*40*).

The *StGAME15* and *PGA1* (*StGAME8*) knockout potato hairy roots were individually generated through targeted genome editing using the CRISPR-Cas9 system. We used the CRISPR-Cas9 binary vector pMgP237-2A-GFP to express multiplex gRNAs (*42*). To design a gRNA target with low off-target effect in *StGAME15* and *PGA1* (*StGAME8*), we conducted in silico analyses using the Web tool Design sgRNAs for CRISPRko (https://portals.broadinstitute.org/gpp/public/analysis-tools/sgrna-design) and Cas-OT software (*43*). We selected target sequences in the coding region. A DNA fragments composed of the gRNA scaffold and tRNA scaffold between two target sequences, were generated by polymerase chain reaction (PCR) using pMD-gtRNA containing gRNA and tRNA scaffolds as a template and primer sets containing restriction enzyme BsaI sites. The gRNAs-tRNAs unit was then inserted into the BsaI site of pMgP237-2A-GFP using Golden Gate Cloning methods to construct the CRISPR-Cas9 vectors. The vectors were introduced into *Agrobacterium rhizogenes* ATC15834 by electroporation. Transgenic potato hairy roots were generated as previously described (*44*). *PGA1i* potato plants were generated previously by Umemoto *et al.* (*21*).

The freeze-dried transformed hairy roots and leaves of the transgenic potatoes were crushed, and 50 mg of each sample was extracted three times with 3 ml of methanol. The extracting solution was evaporated, and the residue was dissolved in 300 µl of methanol and then filtrated with a 0.2 µm PTFE filter (Waters) and subjected to LC-MS/MS analysis. The LC-MS system (Waters) consisted of an AQUITY UPLC (ultraperformance liquid chromatography) H-Class System and an AQUITY quadruple tandem mass spectrometer (TQ detector). MassLynx 4.1 software (Waters) was used to perform data acquisition and analyses. Each sample was injected into an ACQUITY UPLC BEH C18 (1.7 µm 2.1×100 mm Column; Waters), with a column temperature of 40°C and a flow rate of 0.2 ml min^{-1}. The mass spectrometer was operated in the positive electrospray ionization (ESI) mode. For CHR-GlcA detection, the mobile phase consisted of solvent A (3 mM ammonium formate in water) and solvent B (3 mM ammonium formate in 95% acetonitrile), and the following gradient condition was used: 80% B at 0 min, ramped to 100% B at 20 min, held for 25 min, returned to 10% B after 25 min, and held for 30 min. The mass spectrometer was operated in the positive ESI mode. The capillary voltage was 3 kV, source temperature was 120°C, and desolvation gas temperature was 350°C. The nebulizer and desolvation N_2 gas flow rates were 50 and 600 liters hour^{-1}, respectively. Fragmentation was performed using collision-induced dissociation with argon at 0.1 ml min^{-1}. Multiple reaction monitoring (MRM) mode was used. The MRM transition of m/z 580 > 369 with a sample cone voltage of 30 V and a collision energy of 15 eV was used. For the detection of hydroxycholesterol-GlcA, the solvent conditions and MRM channels were modified from the above. The mobile phase consisted of solvent A (0.1% formic acid in water) and solvent B (acetonitrile), and the following gradient condition was used: 20% B at 0 min, ramped to 50% B at 50 min, 100% B at 51 min, held for 56 min, returned to 20% B after 56 min, and held for 61 min. The MRM transition of m/z 596 > 385 with a sample cone voltage of 30 V and a collision energy of 15 eV was used for 22-hydroxycholedterol-GlcA detection and m/z 612 > 401 with a sample cone voltage of 30 V and a collision energy of 15 eV was used for 22,26-dihydroxycholedterol-GlcA detection.

In vivo yeast assay

The cholesterol-producing yeast strain, T41 was constructed from BY4742 *erg6* (*MATα his3D1 leu2D0 lys2D0 ura3D0 erg6::KanMX4*, Open Biosystems) with plasmids pTochigi221-StDWF5 [*LYS2 TDH3*p/*StDWF5*] and pTochigi102-SSR2 [*HIS3 PGK*p/*SSR2*] (*45*). The T41 were transformed with plasmid pESC-LEU-AtUGD2-StCSLM [*LEU2 GAL10*p/*AtUGD2*; *GAL1*p/*StGAME15*] to generate T64. The T64 were transformed with plasmid pESC-URA-StCPR-PGA2 [*URA3 GAL10*p/*StCPR*; *GAL1*p/*PGA2*] to generate T68. Transformants were selected on yeast synthetic medium (SM) with or without lysine, leucine, uracil, and histidine. Each strain was inoculated into the corresponding 5 ml of SM containing 2% glucose and precultured at 30°C for 24 hours at 150 rpm. Yeast cells were pelleted by centrifugation, resuspended in 10 ml of the corresponding 5 ml of SM containing 2% galactose for induction and incubated at 30°C for 2 days at 150 rpm.

Expression of tomato GAME genes in S. cerevisiae WAT11 and metabolite extraction

The pESC constructs were introduced into *S. cerevisiae* WAT11, which expresses cytochrome reductase from *Arabidopsis*, using the Yeastmaker yeast transformation system (Clontech). We transformed yeast cells with various combinations of pESC vectors allowing the expression of one (*GAME15*, *GAME6*, or *GAME8*), two (*GAME15+UGD1*), or three genes (*GAME15+UGD1 +GAME6* or *GAME15+UGD1+GAME8*). The transformed yeast cells were cultivated on synthetic defined (SD) minimal media supplemented with appropriate amino acids and 2% glucose. Colonies were screened, and the presence of the transgene was confirmed by colony PCR. For the induction of gene expression, transformed cells were transferred to minimal medium with 2% galactose (3 ml) and supplemented either with cholesterol or labeled cholesterol-*d*7 [30 µl of substrate, C = 1 mg ml^{-1} in ethanol (EtOH)], and incubated for 48 hours at 30°C. The cultures were then centrifuged for 10 min at 700*g*, the pellet was resuspended in 1 ml of H_2O, transferred to a

2 ml Eppendorf tube, and centrifuged again at 8000g for 1 min. The cell pellet was weighed, and an equal amount of ethanol and double the amount of glass beads (diameter 500 μm) were added. The tubes were placed in a bead beater for 5 min at 22 Hz (RETSCH MM 400 Mixer Mill). The lysed cells were centrifuged at 14,000 rpm for 10 min, the clear supernatant was collected, filtered through a 0.22 μm filter, and analyzed using LC-MS.

In vitro and in vivo assay using insect cells

The DNA fragments containing the open reading frame (ORF) of the StGAME15 and PGA2 (StGAE6) gene were ligated into a pFastBac1 vector (Invitrogen, Carlsbad, CA), and were then introduced into *Escherichia coli* DH10Bac (Life Technologies) to generate the corresponding recombinant bacmid DNAs. Preparation of the recombinant baculoviral DNAs and transfection of *Spodoptera frugiperda 9* insect cells were carried out according to the manufacturer's instructions (Life Technologies). Heterologous expression of StGAME15 and PGA2 (StGAE6) proteins in insect cells was conducted as described by Ohnishi *et al.* (*46*). The culture cells were harvested by centrifugation at 4°C, 1000 ×g for 10 min. The resulting pellet was resuspended in 1 ml of phosphate-buffered saline (PBS) buffer, and after centrifugation at 4°C, 1000 ×g for 2 min, the supernatant was removed to rinse the cells. This rinsing process was repeated three times. The cell pellets were resuspended to 500 μl of MeOH and then centrifuged at 15,000 rpm for 5 min. The supernatant was collected. This MeOH extraction step was repeated three times. The yielding solution was dried and dissolved in 200 μl of MeOH. Each sample was filtered using a 0.2 μm PTFE filter (Waters) and subjected to LC-MS/MS analysis under the conditions described above. In the case of in vitro assay, the culture was centrifuged at 15,000 rpm for 10 min at 4°C, and the cell pellets were resuspended in 250 μl of cold buffer A composed of 50 mM Bis-Tris-HCl (pH7.5), 150 mM NaCl, 10% (v/v) glycerol, and 0.1 mM dithiothreitol. The solution was then sonicated three times for 30 s each on ice using a Bandelin Sonopuls HD 2070 ultrasonic homogenizer type MS73 (Sigma-Aldrich), at a sound intensity of 200 W cm^{-2} and centrifuged at 15,000 rpm for an hour at 4°C. The supernatant was removed, and the pellet fraction was resuspended in 250 μl of buffer A. This suspension was used as the membrane fraction for the in vitro assay. An in vitro enzyme activity assay was performed using 100 μl of reaction mixture containing 50 mM Tris-HCl (pH 7.5), 1 mM MgCl$_2$, 6.2 mM UDP-GlcA, 25 μM substrate, and 50 μl of membrane fraction suspension. The reaction was initiated by the addition of the enzyme and was carried out at 30°C for 24 hours. 100 μl of EtOAc was added to the reaction mixture, vortexed, and

then centrifuged at 15,000 rpm for 1 min to collect the upper layer. This process was repeated three times. After this EtOAc extraction, the sample solution was dried and dissolved in 150 μl of MeOH. Each sample was filtered through a 0.2 μm PTFE filter (Waters) and subjected to LC-MS/MS analysis under the conditions described above.

Molecular biology and transient assays in N. benthamiana

Genes of interest were amplified by PCR from tomato or *L. muscari* cDNA using primers listed in table S3. PrimeSTAR GXL DNA Polymerase (Takara Bio) was used for gene amplification. Tomato GAME genes were cloned into pDBG3α1 or pDBG3α2 vectors using GoldenBraid cloning system (*47*). *Liriope* genes were directly cloned into pDBG3α1 vector using the One Step Cloning Kit (C112-02, Vazyme) according to the manufacturer's instructions.

Constructs were transformed into *Agrobacterium tumafaciens* (GV3101) electrocompetent cells. Transformants were grown on LB plates containing 50 μg ml^{-1} kanamycin and 50 μg ml^{-1} gentamicin at 28°C. Then, 10 ml of LB medium supplemented with antibiotics was inoculated with a single colony and grew O/N at 28°C. Cells were centrifuged at 3000g for 10 min and supernatant removed. Pellet was resuspended in 5 ml of infiltration medium (100 mM MES buffer, 2 mM Na$_3$PO$_4$•12H$_2$O, 100 μM acetosyringone) and centrifuged again. Pellet was resuspended again in 10 ml of infiltration medium and incubated at room temperature for 2 hours. *Agrobacterium* suspensions consisting of one strain or multiple strains [optical density at a wavelength of 600 nm (OD600) = 0.3 for each strain] were infiltrated into the underside of *N. benthamiana* leaves with a needleless 1 ml syringe. Plants were grown for 4 to 5 weeks under a 16-hour light cycle before infiltration. Leaves were harvested 4 days postinfiltration, frozen in liquid nitrogen, and stored at −80°C for later processing. Biological replicates consisted of several leaves all from different tobacco plants.

Construct preparation for VIGS

To achieve the silencing of candidate genes in *S. pennellii*, the following steps were undertaken. First, gene sequences [200 to 400 base pairs (bp)] were amplified from *S. pennellii* leaf cDNA template, and ~200 bp of the *Magnesium Chelatase Subunit H* (*SlCHLH*) was incorporated into an EcoRI-digested pTRV2 vector as a silencing marker. Subsequently, the purified amplicons of candidate genes were introduced into a modified pTRV2 vector, which had been digested with SacI.

The utilization of this pTRV2 plasmid results in the simultaneous silencing of two genes: *SlCHLH* (inducing a chlorotic phenotype and functioning as a silencing marker) and

the candidate gene that was silenced in the same plant region as *CHLH*. This strategic approach enables the collection of tissue in which the candidate gene has been successfully silenced.

Phylogenetic analysis

Phylogenetic analysis of cellulose synthase–like enzymes was performed as described previously (*28*). The phylogenetic tree was visualized with iTOL (*48*).

Quantitative reverse transcription PCR (qRT-PCR) analysis

Gene expression analysis was performed as described previously (*49*).

MALDI imaging

MALDI imaging was performed as described in Polturak *et al.* (*50*).

Metabolite extraction
Extraction of SGAs

Briefly, 100 mg of frozen powdered plant tissue was extracted with 300 μl of 80% methanol + 0.1% formic acid, briefly vortexed and then sonicated for 20 min at room temperature. Extracts were centrifuged for 10 min at 14,000g and filtered through 0.22 μm filters. At least three biological replicates ($n = 3$) from sample were used for metabolic analysis.

Extraction of tomatidine, hydroxycholesterols, and diosgenin or yamogenin

Four leaf discs (diameter = 8 mm) were collected from two different tobacco leaves, placed in a 2 ml tube together with two metal balls, and snap-frozen in liquid nitrogen. Tissues were powdered using bead beater for 2 min at 22 Hz (RETSCH MM 400 Mixer Mill). Ground tissue was mixed with 0.5 ml of 20% KOH in 50% EtOH, briefly vortexed, and incubated at 65°C for 1 hour. Each sample was extracted three times with 0.6 ml of hexane. Pooled hexane fractions were evaporated, and residue was resuspended in 0.1 ml of EtOH. Samples were analyzed on the LC-MS on the same day.

Sterol extraction for GC-MS analysis

Sterol extraction was performed as described previously (*33*).

Extraction of sterols and sterol glucosides for LC-MS analysis

One hundred milligrams of frozen ground leaf tissue powder was extracted 400 μl of ethanol, briefly vortexed, and then sonicated for 20 min at room temperature. Extracts were centrifuged for 10 min at 14,000g and filtered through 0.22 μm filters. At least three biological replicates ($n = 3$) from sample were used for metabolic analysis.

Acid hydrolysis of 22-hydroxy and 26-hydroxycholesterol-GlcA

Plant extracts (500 µl) containing GlcA derivatives of hydroxylated cholesterol (products of GAME15 and GAME6 or GAME8 activity on cholesterol) were dried in a SpeedVac at room temperature. The dry residue was resuspended in 500 µl of 2 M HCl in 50% MeOH, vortexed thoroughly, and incubated for 1 hour at 70°C. After cooling, 250 µl of 4 M NaOH solution was added to neutralize the pH. Hydroxysterols were then extracted three times with 500 µl of hexane. The pooled hexane extracts were dried under a stream of nitrogen, dissolved in 100 µl of EtOH, and immediately analyzed by LC-MS. Metabolite identity was confirmed using commercial standards for 22S-hydroxycholesterol, 22R-hydroxycholesterol, and 26-hydroxycholesterol.

Metabolic profiling

LC-MS was performed on a Xevo TQS quadrupole mass spectrometer (Waters) coupled to an ACQUITY UPLC system (Waters). A SYNAPT-G2 quadrupole time-of-flight (qTOF) mass spectrometer (Waters) coupled to ACQUITY UPLC system (Waters) was used for liquid chromatography–high-resolution mass spectrometry (LC-HRMS) analysis. MassLynx software v.4.1 (Waters) was used to control the instrument and calculate accurate masses and elemental compositions.

Separation of metabolites (SGAs, hydroxysterols, tomatidine, and diosgenin or yamogenin) was performed on a 100 mm × 2.1 mm i.d. (internal diameter), 1.7 µm UPLC BEH C18 column (Waters Acquity). The mobile phase consisted of 0.1% formic acid in acetonitrile:water (5:95, v/v; phase A) and 0.1% formic acid in acetonitrile (phase B). The flow rate was 0.3 ml min^{-1}, and the column temperature was kept at 35°C.

SGA analysis in WT and GAME15i tomatoes

SGA content was analyzed as described previously by Itkin et al. ([20]).

LC-MS conditions used to analyze hydroxysterols and diosgenin or yamogenin

The following linear gradient was used for analysis of hydroxysterols and diosgenin or yamogenin: from 60 to 0% phase A over 10 min, then held at 100% phase B for 7 min; and then returned to the initial conditions (60% phase A) within 0.5 min and conditioning at 60% phase A for 2.5 min.

LC-MS conditions used to analyze tomatidenol and tomatidine

The following linear gradient was used for analysis of tomatidenol and tomatidine in N. benthamiana agroinfiltrated leaves: from 85 to 55% phase A over 13 min, from 55% to 0% A over 0.5 min, then held at 100% phase B for 3.5 min; and then returned to the initial conditions (85% phase A) within 0.5 min and conditioning at 85% phase A for 2.5 min.

LC-MS conditions used to analyze sterol glucosides

The following linear gradient was used for analysis of sterol glucosides from WT and GAME15i tomato lines: from 50% to 15% phase A (1% ACN in water) over 5 min, from 15% to 0% A over 20 min, then held at 100% phase B (MeOH) for 10 min; and then returned to the initial conditions (50% phase A) within 1 min and conditioning at 50% phase A for 4 min. Flow was kept at 0.2 ml min^{-1}.

MS settings

High-resolution mass measurements were performed on Synapt-G2 operated in full-scan mode (m/z range: 50 to 1600) with the following parameters: capillary, 1.5 kV; source temperature, 140°C; sampling cone, 20 V; desolvation temperature, 450°C; cone gas flow, 53 liters hour^{-1}; desolvation gas flow, 800.0 liters hour^{-1}; nebulizer gas flow, 7.0 bar; trap collision energy, 4.0 V.

For LC-MS analysis, Xevo TQS quadrupole mass spectrometer was configured to perform MRM scans with the following parameters: capillary, 3.0 kV; source temperature, 150°C; sampling cone, 20 V; desolvation temperature, 350°C; cone gas flow, 150 liters hour^{-1}; desolvation gas flow, 650.0 liters hour^{-1}; nebulizer gas flow, 7.0 bar. Hydroxycholesterols: MRM1: 385.34 > 257.35, collision energy 20.0; MRM2: 385.34 > 367.33, collision energy 12.0. Diosgenin or yamogenin: MRM1: 415.32 > 253.30, collision energy 22.0; MRM2: 415.32 > 271.30, collision energy 16.0. Tomatidenol: MRM1: 414.30 > 253.25, collision energy 25.0; MRM2: 414.30 > 271.20, collision energy 25.0. Tomatidine: MRM1: 416.40 > 255.25, collision energy 25.0; MRM2: 416.40 > 273.30, collision energy 25.0. Tomatidenol-$d6$: MRM1: 420.40 > 258.25, collision energy 25.0; MRM2: 420.40 > 277.20, collision energy 25.0.

Metabolites were identified by comparing the retention times and mass fragments of standard compounds. Relative quantification of metabolites was carried out using the TargetLynx (Waters) program.

Confocal microscopy and subcellular localization

Plasmids enabling the expression of the target proteins fused with fluorescent proteins were constructed using the One Step Cloning Kit (C112-02, Vazyme). While combining gene of interest with a fluorescent protein, we used a flexible 10–amino acid linker (GlyGlyGlyGlySer × 2). For cell compartment labeling, plasmids sourced from ABRC (ER-gk CD3-955 and G-gk CD3-963) were used. To investigate the subcellular localization of tomato GAME15, GAME15:mRFP was transiently expressed alongside an ER or Golgi marker in N. benthamiana epidermal cells. Each Agrobacterium strain was infiltrated using a bacterial absorbance A600 nm of 0.15. After a 72-hour postinfiltration period,

leaf disks (~0.4-cm diameter) were harvested and subjected to fluorescence analysis using confocal microscopy. The Nikon Eclipse A1 microscope with a 488 nm laser for excitation was used, capturing images for GFP (ER or Golgi marker) and 561 nm for RFP signals. To enhance the signal-to-noise ratio, each scan pixel was sampled four times and averaged. The same parameters were applied to assess the colocalization of other GAME proteins.

Split-LUC assay

Split luciferase complementation imaging assays were performed according to the method described by Cai et al. ([51]).

In planta FLIM to determine FRET efficiency

The samples (whole leaf discs) were prepared 4 days postinfiltration and mounted with water. Mounting slides were closed with cover glass thickness No. 1 and sealed with silicon to prevent drying and movement of the leaf disc. Confocal imaging was performed using an inverted Leica SP8 STED3X microscope, equipped with internal Hybrid (HyD) detectors and Acusto Optical Tunable Filter (Leica microsystems CMS GmbH, Germany) and the white light laser (WLL) excitation laser ranging from 470 to 670 nm. eGFP and mRFP1 excitation was performed using a pulsed WLL, 488 nm and 561 nm, 40 MHz frequency at 2% laser power. The emission signal was collected using two internal HyD detectors in the range of 498 to 550 nm and 590 to 650 nm. Images were acquired using the galvometric scanner in the format of 256x256 with HC PL APO 63x/1.20 W CORR CS2 objective lens (506346 Leica microsystems CMS GmbH, Germany). Scan Speed was 400 Hz, pinhole 1 airy unit at 580 nm (11.5 µm), and bit depth was 8. The images were acquired in Leica Application Suite LAS X FLIM–fluorescence correlation spectroscopy (FCS) mode, version 3.5.6. For each condition, measurements were done on 30 independent images. Accumulation was set to a maximum photon count of 500 and the selected fit model was set to "n-Exponential Reconvolution." The exponential components were set to 2. Mean τ intensity weighed (ns) was calculated from the fully acquired image in the Leica Application Suite LAS X FLIM-FCS mode. To calculate average FRET efficiency, mean τ intensity weighed (n) was placed in the following formula

$$\text{FRET efficiency} = 1 - \left(\frac{\tau \text{ASSAY}}{\tau \text{ALONE}}\right)$$
$$= \left(\frac{R_0^6}{R_0^6 + R}\right)$$

with R_0 the Förster radius, R the distance between donor and acceptor, τASSAY the lifetime of the donor in the presence of the acceptor,

and τALONE the lifetime of the donor in the absence of acceptor. Standard deviation was calculated as follows

$$\text{SD FRET} = \%\text{FRET}$$
$$\sqrt{\left(\frac{\text{SD ASSAY}}{\text{Average ASSAY}}\right)^2 + \left(\frac{\text{SD ALONE}}{\text{Average ALONE}}\right)^2}$$

TAP-MS

Affinity purification of GAME15 tagged with GFP and its interactors was performed using Pull down Miltenyi microMACs GFP kit following previously described protocol ([52]). All the steps were performed at 4ºC, on ice and in the cold room, unless otherwise stated. One hundred to 200 mg of ground tissue were mixed with 1 ml of lysis buffer (150 mM NaCl, 1% Ecosurf EH-9, 50 mM Tris HCl, pH 8.0) supplemented with 1% of protease inhibitor cocktail (Sigma-Aldrich) kept on ice and vortex regularly. To remove cell debris, lysate was centrifuged three times at 14,000 rpm for 10 min each time. 50 μl of anti-GFP microbeads was added and kept for 30 min on ice and vortexed regularly. μColumns (Miltenyi biotech) were placed on the magnetic rack and activated with 200 μl of lysis buffer supplemented with protease inhibitor. Samples were loaded on the columns and washed four times with 200 μl of wash buffer 1 (150 mM NaCl, 1% Ecosurf EH-9, 0.5% sodium deoxycholate, 0.1% SDS, 50 mM Tris HCl, pH 8.0), and once with 100 μl of wash buffer 2 (20 mM Tris HCl pH 7.5). Proteins were eluted with 50 μl of elution buffer into clean Eppendorf tube. Samples for proteomic analysis were prepared following previously described modified filter-aided sample preparation protocol (FASP) ([34]). Peptides were acidified with trifluoroacetic acid, dried in a Speedvac concentrator and analyzed using nano-UPLC (Waters, Milford, MA, USA), coupled to a nano-ESI emitter (10 μM tip; New Objective, Cambridge, MA, USA) and to a quadrupole Orbitrap mass spectrometer (Q Exactive Plus; Thermo Scientific, Bremen, Germany) as described in Szymanski et al. ([53]). Protein identification and label-free quantification was performed using Proteome Discoverer software (v.2.2) (Thermo Fisher Scientific). The following parameters were set for searching the Sequest HT engine against the ITAG 4.1 and Niben101 databases (SGN): (i) maximum two missed tryptic cleavages; (ii) precursor mass tolerance 10 ppm; (iii) fragment mass tolerance 0.02 Da; and (iv) fixed and variable modifications, such as carbamidomethylation of Cys and oxidation of Met. The data were filtered for a minimum of two peptides matching the protein and false discovery rate (FDR) value of ≤0.01 (both for protein and peptide).

Metabolite channeling analysis

Leaves of N. benthamiana transiently expressing GAME enzymes were infiltrated with labeled precursor of the SGA pathway, [^{2}H$_6$]cholesterol. Infiltration media consisting of 50 mM MES, 2 mM Na$_3$PO$_4$, 28 mM glucose, 1% Tween-20, and 25 uM cholesterol-d6 was used to deliver the substrate to the plant. After 3 days, leaf tissue was collected, ground in liquid nitrogen, and extracted, as described above (tomatidine extraction protocol). Samples were analyzed using LC-TQ-MS working in MRM mode, as described before.

Insect assay

S. littoralis (Egyptian cotton leafworm) growth and feeding experiment was done as described previously ([54]).

REFERENCES AND NOTES

1. M. Pröschel, R. Detsch, A. R. Boccaccini, U. Sonnewald, Engineering of Metabolic Pathways by Artificial Enzyme Channels. Front. Bioeng. Biotechnol. 3, 168 (2015). doi: 10.3389/fbioe.2015.00168; pmid: 26557643

2. J. B. Robinson Jr., P. A. Srere, Organization of Krebs tricarboxylic acid cycle enzymes in mitochondria. J. Biol. Chem. 260, 10800–10805 (1985). doi: 10.1016/S0021-9258(19)85153-0; pmid: 4030772

3. A. R. Fernie, Y. Zhang, L. J. Sweetlove, Passing the Baton: Substrate Channelling in Respiratory Metabolism. Research 2018, 1539325 (2018). doi: 10.1155/2018/1539325; pmid: 31549022

4. J. W. A. Graham et al., Glycolytic enzymes associate dynamically with mitochondria in response to respiratory demand and support substrate channeling. Plant Cell 19, 3723–3738 (2007). doi: 10.1105/tpc.107.053371; pmid: 17981998

5. E. Puchulu-Campanella et al., Identification of the components of a glycolytic enzyme metabolon on the human red blood cell membrane. J. Biol. Chem. 288, 848–858 (2013). doi: 10.1074/jbc.M112.428573; pmid: 23150667

6. D. Araiza-Olivera et al., A glycolytic metabolon in Saccharomyces cerevisiae is stabilized by F-actin. FEBS J. 280, 3887–3905 (2013). doi: 10.1111/febs.12387; pmid: 23763840

7. M. M. Islam et al., Branched-chain amino acid metabolon: Interaction of glutamate dehydrogenase with the mitochondrial branched-chain aminotransferase (BCATm). J. Biol. Chem. 285, 265–276 (2010). doi: 10.1074/jbc.M109.048777; pmid: 19858196

8. M. Panicot et al., A polyamine metabolon involving aminopropyl transferase complexes in Arabidopsis. Plant Cell 14, 2539–2551 (2002). doi: 10.1105/tpc.004077; pmid: 12368503

9. A. Stavrinides et al., Unlocking the diversity of alkaloids in Catharanthus roseus: Nuclear localization suggests metabolic channeling in secondary metabolism. Chem. Biol. 22, 336–341 (2015). doi: 10.1016/j.chembiol.2015.02.006; pmid: 25772467

10. T. Laursen et al., Characterization of a dynamic metabolon producing the defense compound dhurrin in sorghum. Science 354, 890–893 (2016). doi: 10.1126/science.aag2347; pmid: 27856908

11. N. Fujino et al., Physical interactions among flavonoid enzymes in snapdragon and torenia reveal the diversity in the flavonoid metabolon organization of different plant species. Plant J. 94, 372–392 (2018). doi: 10.1111/tpj.13864; pmid: 29421843

12. M. Gou, X. Ran, D. W. Martin, C.-J. Liu, The scaffold proteins of lignin biosynthetic cytochrome P450 enzymes. Nat. Plants 4, 299–310 (2018). doi: 10.1038/s41477-018-0142-9; pmid: 29725099

13. M. Camagna et al., Enzyme Fusion Removes Competition for Geranylgeranyl Diphosphate in Carotenogenesis. Plant Physiol. 179, 1013–1027 (2019). doi: 10.1104/pp.18.01026; pmid: 30309967

14. S. Mucha et al., The Formation of a Camalexin Biosynthetic Metabolon. Plant Cell 31, 2697–2710 (2019). doi: 10.1105/tpc.19.00403; pmid: 31511315

15. Y. Zhang, A. R. Fernie, Metabolons, enzyme-enzyme assemblies that mediate substrate channeling, and their roles in plant metabolism. Plant Commun. 2, 100081 (2020). doi: 10.1016/j.xplc.2020.100081; pmid: 33511342

16. R. P. Bhattacharyya, A. Reményi, B. J. Yeh, W. A. Lim, Domains, motifs, and scaffolds: The role of modular interactions in the evolution and wiring of cell signaling circuits. Annu. Rev. Biochem. 75, 655–680 (2006). doi: 10.1146/annurev.biochem.75.103004.142710; pmid: 16756506

17. M. C. Good, J. G. Zalatan, W. A. Lim, Scaffold proteins: Hubs for controlling the flow of cellular information. Science 332, 680–686 (2011). doi: 10.1126/science.1198701; pmid: 21551057

18. M. I. Page, W. P. Jencks, Entropic contributions to rate accelerations in enzymic and intramolecular reactions and the chelate effect. Proc. Natl. Acad. Sci. U.S.A. 68, 1678–1683 (1971). doi: 10.1073/pnas.68.8.1678; pmid: 5288752

19. M. Itkin et al., Biosynthesis of antinutritional alkaloids in solanaceous crops is mediated by clustered genes. Science 341, 175–179 (2013). doi: 10.1126/science.1240230; pmid: 23788733

20. M. Itkin et al., GLYCOALKALOID METABOLISM1 is required for steroidal alkaloid glycosylation and prevention of phytotoxicity in tomato. Plant Cell 23, 4507–4525 (2011). doi: 10.1105/tpc.111.088732; pmid: 22180624

21. N. Umemoto et al., Two Cytochrome P450 Monooxygenases Catalyze Early Hydroxylation Steps in the Potato Steroid Glycoalkaloid Biosynthetic Pathway. Plant Physiol. 171, 2458–2467 (2016). doi: 10.1104/pp.16.00137; pmid: 27307258

22. M. Nakayasu et al., A Dioxygenase Catalyzes Steroid 16α-Hydroxylation in Steroidal Glycoalkaloid Biosynthesis. Plant Physiol. 175, 120–133 (2017). doi: 10.1104/pp.17.00501; pmid: 28754839

23. C. P. Moehs, P. V. Allen, M. Friedman, W. R. Belknap, Cloning and expression of solanidine UDP-glucose glucosyltransferase from potato. Plant J. 11, 227–236 (1997). doi: 10.1046/j.1365-313X.1997.11020227.x; pmid: 9076990

24. K. F. McCue et al., Metabolic compensation of steroidal glycoalkaloid biosynthesis in transgenic potato tubers: Using reverse genetics to confirm the in vivo enzyme function of a steroidal alkaloid galactosyltransferase. Plant Sci. 168, 267–273 (2005). doi: 10.1016/j.plantsci.2004.08.006

25. K. F. McCue et al., The primary in vivo steroidal alkaloid glucosyltransferase from potato. Phytochemistry 67, 1590–1597 (2006). doi: 10.1016/j.phytochem.2005.09.037; pmid: 16298403

26. K. F. McCue et al., Potato glycosterol rhamnosyltransferase, the terminal step in triose side-chain biosynthesis. Phytochemistry 68, 327–334 (2007). doi: 10.1016/j.phytochem.2006.10.025; pmid: 17157337

27. R. Akiyama et al., The biosynthetic pathway of potato solanidanes diverged from that of spirosolanes due to evolution of a dioxygenase. Nat. Commun. 12, 1300 (2021). doi: 10.1038/s41467-021-21546-0; pmid: 33637735

28. A. Jozwiak et al., Plant terpenoid metabolism co-opts a component of the cell wall biosynthesis machinery. Nat. Chem. Biol. 16, 740–748 (2020). doi: 10.1038/s41589-020-0541-x; pmid: 32424305

29. S. Y. Chung et al., A cellulose synthase-derived enzyme catalyses 3-O-glucuronosylation in saponin biosynthesis. Nat. Commun. 11, 5664 (2020). doi: 10.1038/s41467-020-19399-0; pmid: 33199711

30. M. M. Augustin et al., Elucidating steroid alkaloid biosynthesis in Veratrum californicum: Production of verazine in Sf9 cells. Plant J. 82, 991–1003 (2015). doi: 10.1111/tpj.12871; pmid: 25939370

31. B. Christ et al., Repeated evolution of cytochrome P450-mediated spiroketal steroid biosynthesis in plants. Nat. Commun. 10, 3206 (2019). doi: 10.1038/s41467-019-11286-7; pmid: 31324795

32. C. Zhou et al., 22R- but not 22S-hydroxycholesterol is recruited for diosgenin biosynthesis. Plant J. 109, 940–951 (2022). doi: 10.1111/tpj.15604; pmid: 34816537

33. P. D. Sonawane et al., Plant cholesterol biosynthetic pathway overlaps with phytosterol metabolism. Nat. Plants 3, 16205 (2016). doi: 10.1038/nplants.2016.205; pmid: 28005066

34. Y. Kazachkova et al., The GORKY glycoalkaloid transporter is indispensable for preventing tomato bitterness. Nat. Plants 7, 468–480 (2021). doi: 10.1038/s41477-021-00865-6; pmid: 33707737

35. L. Beste et al., Synthesis of hydroxylated sterols in transgenic Arabidopsis plants alters growth and steroid metabolism. Plant Physiol. 157, 426–440 (2011). doi: 10.1104/pp.110.171199; pmid: 21746809

36. T. Louveau, A. Osbourn, The Sweet Side of Plant-Specialized Metabolism. Cold Spring Harb. Perspect. Biol. 11, a034744 (2019). doi: 10.1101/cshperspect.a034744; pmid: 31235546

37. K. Ramirez-Estrada et al., Tomato UDP-Glucose Sterol Glycosyltransferases: A Family of Developmental and Stress Regulated Genes that Encode Cytosolic and Membrane-Associated

Forms of the Enzyme. *Front. Plant Sci.* **8**, 984 (2017). doi: 10.3389/fpls.2017.00984; pmid: 28649260

38. P. Heinz, M. A. Glomb, Characterization and Quantitation of Steryl Glycosides in *Solanum melongena*. *J. Agric. Food Chem.* **66**, 11398–11406 (2018). doi: 10.1021/acs.jafc.8b04045; pmid: 30336036

39. P. D. Cárdenas *et al.*, GAME9 regulates the biosynthesis of steroidal alkaloids and upstream isoprenoids in the plant mevalonate pathway. *Nat. Commun.* **7**, 10654 (2016). doi: 10.1038/ncomms10654; pmid: 26876023

40. P. D. Sonawane *et al.*, A BAHD-type acyltransferase concludes the biosynthetic pathway of non-bitter glycoalkaloids in ripe tomato fruit. *Nat. Commun.* **14**, 4540 (2023). doi: 10.1038/s41467-023-40092-5; pmid: 37500644

41. M. Omary *et al.*, A conserved superlocus regulates above- and belowground root initiation. *Science* **375**, eabf4368 (2022). doi: 10.1126/science.abf4368; pmid: 35239373

42. R. Hashimoto, R. Ueta, C. Abe, Y. Osakabe, K. Osakabe, Efficient Multiplex Genome Editing Induces Precise, and Self-Ligated Type Mutations in Tomato Plants. *Front. Plant Sci.* **9**, 916 (2018). doi: 10.3389/fpls.2018.00916; pmid: 30018630

43. A. Xiao *et al.*, CasOT: A genome-wide Cas9/gRNA off-target searching tool. *Bioinformatics* **30**, 1180–1182 (2014). doi: 10.1093/bioinformatics/btt764; pmid: 24389662

44. M. Nakayasu *et al.*, Generation of α-solanine-free hairy roots of potato by CRISPR/Cas9 mediated genome editing of the *St16DOX* gene. *Plant Physiol. Biochem.* **131**, 70–77 (2018). doi: 10.1016/j.plaphy.2018.04.026; pmid: 29735370

45. S. Sawai *et al.*, Sterol side chain reductase 2 is a key enzyme in the biosynthesis of cholesterol, the common precursor of toxic steroidal glycoalkaloids in potato. *Plant Cell* **26**, 3763–3774 (2014). doi: 10.1105/tpc.114.130096; pmid: 25217510

46. T. Ohnishi *et al.*, C-23 hydroxylation by *Arabidopsis* CYP90C1 and CYP90D1 reveals a novel shortcut in brassinosteroid biosynthesis. *Plant Cell* **18**, 3275–3288 (2006). doi: 10.1105/tpc.106.045443; pmid: 17138693

47. M. Vazquez-Vilar *et al.*, GB3.0: A platform for plant bio-design that connects functional DNA elements with associated biological data. *Nucleic Acids Res.* **45**, 2196–2209 (2017). doi: 10.1093/nar/gkw1326; pmid: 28053117

48. I. Letunic, P. Bork, Interactive Tree Of Life (iTOL) v5: An online tool for phylogenetic tree display and annotation. *Nucleic Acids Res.* **49**, W293–W296 (2021). doi: 10.1093/nar/gkab301; pmid: 33885785

49. S. Panda *et al.*, Steroidal alkaloids defence metabolism and plant growth are modulated by the joint action of gibberellin and jasmonate signalling. *New Phytol.* **233**, 1220–1237 (2022). doi: 10.1111/nph.17845; pmid: 34758118

50. G. Polturak *et al.*, Engineered gray mold resistance, antioxidant capacity, and pigmentation in betalain-producing crops and ornamentals. *Proc. Natl. Acad. Sci. U.S.A.* **114**, 9062–9067 (2017). doi: 10.1073/pnas.1707176114; pmid: 28760998

51. J. Cai, G. Qin, T. Chen, S. Tian, The mode of action of remorin1 in regulating fruit ripening at transcriptional and post-transcriptional levels. *New Phytol.* **219**, 1406–1420 (2018). doi: 10.1111/nph.15264; pmid: 29978907

52. L. C. Noack *et al.*, A nanodomain-anchored scaffolding complex is required for the function and localization of phosphatidylinositol 4-kinase alpha in plants. *Plant Cell* **34**, 302–332 (2022). doi: 10.1093/plcell/koab135; pmid: 34010411

53. J. Szymanski *et al.*, Label-free deep shotgun proteomics reveals protein dynamics during tomato fruit tissues development. *Plant J.* **90**, 396–417 (2017). doi: 10.1111/tpj.13490; pmid: 28112434

54. B. Negin *et al.*, Fatty alcohols, a minor component of the tree tobacco surface wax, are associated with defence against caterpillar herbivory. *Plant Cell Environ.* **47**, 664–681 (2024). doi: 10.1111/pce.14752; pmid: 37927215

ACKNOWLEDGMENTS

SUPPLEMENTARY MATERIALS